General Disclaimer

One or more of the Following Statements may affect this Document

- This document has been reproduced from the best copy furnished by the organizational source. It is being released in the interest of making available as much information as possible.

- This document may contain data, which exceeds the sheet parameters. It was furnished in this condition by the organizational source and is the best copy available.

- This document may contain tone-on-tone or color graphs, charts and/or pictures, which have been reproduced in black and white.

- This document is paginated as submitted by the original source.

- Portions of this document are not fully legible due to the historical nature of some of the material. However, it is the best reproduction available from the original submission.

SOLAR MICROCLIMATOLOGY

CONTRACT NO. NASW-2745

FINAL REPORT

NOVEMBER 1975

Prepared For

NASA Headquarters
Washington, D. C. 20546

Prepared By:

Dean B. McKenney
William T. Beauchamp

Approved By:

Dean B. McKenney
Program Manager

HELIO ASSOCIATES, INC.
P.O. Box 17960
Tucson, Arizona 85731

BIBLIOGRAPHIC DATA SHEET	1. Report No.	2.	3. Recipient's Accession No.
4. Title and Subtitle			5. Report Date
"Solar Microclimatology"			November 1975
			6.
7. Author(s) W. T. Beauchamp and D. B. McKenney			8. Performing Organization Rept. No.
9. Performing Organization Name and Address			10. Project/Task/Work Unit No.
Helio Associates, Inc. P. O. Box 17960 Tucson, Arizona 85731			11. Contract/Grant No. NASA 2745
12. Sponsoring Organization Name and Address			13. Type of Report & Period Covered
NASA Headquarters Washington, C. D. 20546			Final Report Nov 1975
			14.

15. Supplementary Notes

16. Abstracts

Insolation data was collected and analyzed for a network of sensors distributed over an area of several square kilometers. The analyses of this data yielded probability distributions of cloud size, velocity, and direction of motion which were compared with data obtained from the National Weather Service. Microclimatological analyses were also performed for suitable modeling parameters pertinent to large scale power plant design.

17. Key Words and Document Analysis. 17a. Descriptors

Solar Energy
Solar Insolation
Solar Power Plant Design
Cloud Motion
Insolation Instrumentation
Insolation Measurements

17b. Identifiers/Open-Ended Terms

ORIGINAL PAGE IS OF POOR QUALITY

17c. COSATI Field/Group

18. Availability Statement	19. Security Class (This Report) UNCLASSIFIED	21. No. of Pages
Release Unlimited	20. Security Class (This Page) UNCLASSIFIED	22. Price

ABSTRACT

Insolation data was collected and analyzed for a network of sensors distributed over an area of several square kilometers. The analyses of this data yielded probability distributions of cloud s̶h̶a̶d̶o̶w̶ ̶s̶i̶z̶e̶,̶ ̶a̶n̶d̶ ̶d̶i̶r̶e̶c̶t̶ion of motion which were compared with data obtained from the National Weather Service. Micro-climatological analyses were also performed for suitable modeling parameters pertinent to large scale power plant design.

TABLE OF CONTENTS

TABLES

SECTION 1.0 INTRODUCTION

It has become apparent in recent years that Solar Energy can be used for electric power production by several methods. Because of the diffuse nature of the solar insolation, the area involved in any central power plant design would encompass several square miles. Detailed design of these large area collection systems will require precise knowledge of the local solar insolation. Information regarding the total available insolation and suitable integrals of the data are currently available with off the shelf instruments and from many National Weather Service installations. However, for many system designs, detailed information will also be needed concerning the temporal nature of the insolation and the local spatial distribution. Such information is not currently available in the literature. Visual observations show that it will be highly probable that different portions of a large - several km across - collecting area will experience different insolation characteristics at different times of the day due to clouds smaller than km dimensions. It will be necessary to take these effects into account in future analyses of solar collector systems.

The purpose of this research project was the collection and analysis of insolation data from a network of sensors distributed over an area several kilometers on a side. Both direct-normal and total-horizontal insolation data were collected in

order to model various solar absorber system types. The field
of detectors used to gather the data formed a 3.6 x 1.6 km grid.
This grid allowed for two independent evaluations of the velocity
and direction of motion for clouds passing overhead. The calcu-
lated velocity was used with the duration of the occultation to
obtain a typical dimension for each cloud. A Fourier modeling
of temporal and spatial distribution of the solar insolation over
the field was also done. A complete discussion of this modeling
and the microclimate trends are presented in the following sec-
tions. A brief summary is presented in the next paragraph.

The data analysis reported here has yielded much valuable
information despite the amount of varience in cloud types observed,
the variety of weather conditions in the area, and the complexity
of the resulting "events". Several interesting features are found
for Tucson's microclimate. These features readily illustrate
the information available for large scale system designs. The
velocities measured for the occulting clouds are principally in
the range from 0.60 km to about 9.7 km with the most probable
extent in the direction of motion of about 0.19 km. The data span
six months of operation and include more than 200 individual
events. About 40% of these events were represented by sufficient
data to calculate two independent values of the velocity and
direction of motion. About 67% of these correlatable events
showed good agreement in both values of the velocity and direc-
tion. This suggests a 67% confidence in any single vector velocity

calculation. The analysis results are discussed in detail in Section 3. A brief review of the instruments and the field layout follows.

SECTION 2.0 FIELD AND INSTRUMENT DESCRIPTION

2.1 Instruments - Physical

The instruments used to specify the solar insolation are modified pyranometers with a shadow bar that interrupts the direct solar beam as it rotates around the detector aperture. A sketch of the Moving Bar Occulting Radiometer (MBOR) is shown in Figure 1. The compact size of this instrument - about 20 x 6.5 x 7 cm - makes it suitable for field operation. A 4.8 mm diameter circular detector aperture is located on the axis of revolution of a circular occulting bar. The surface of the aperture is opal glass. A detector is mounted beneath the aperture plate as shown in Figure 2. The area immediately under the aperture plate houses a neutral density filter required to keep the detectors from saturating at the maximum flux levels. This surface-filter-detector combination insures an output that is a linear function of the flux level and a cosine like angular response. The occulting bar is driven at a rate of $\frac{1}{3}$ RPM, and has a cross section such that a sharp shadow just covers the aperture once per revolution of the bar in the field of view. To minimize the error in the diffuse flux caused by the presence of the bar, its width is specified by

$$w = d + 2R \sin (\tfrac{1}{2}^{\circ})$$
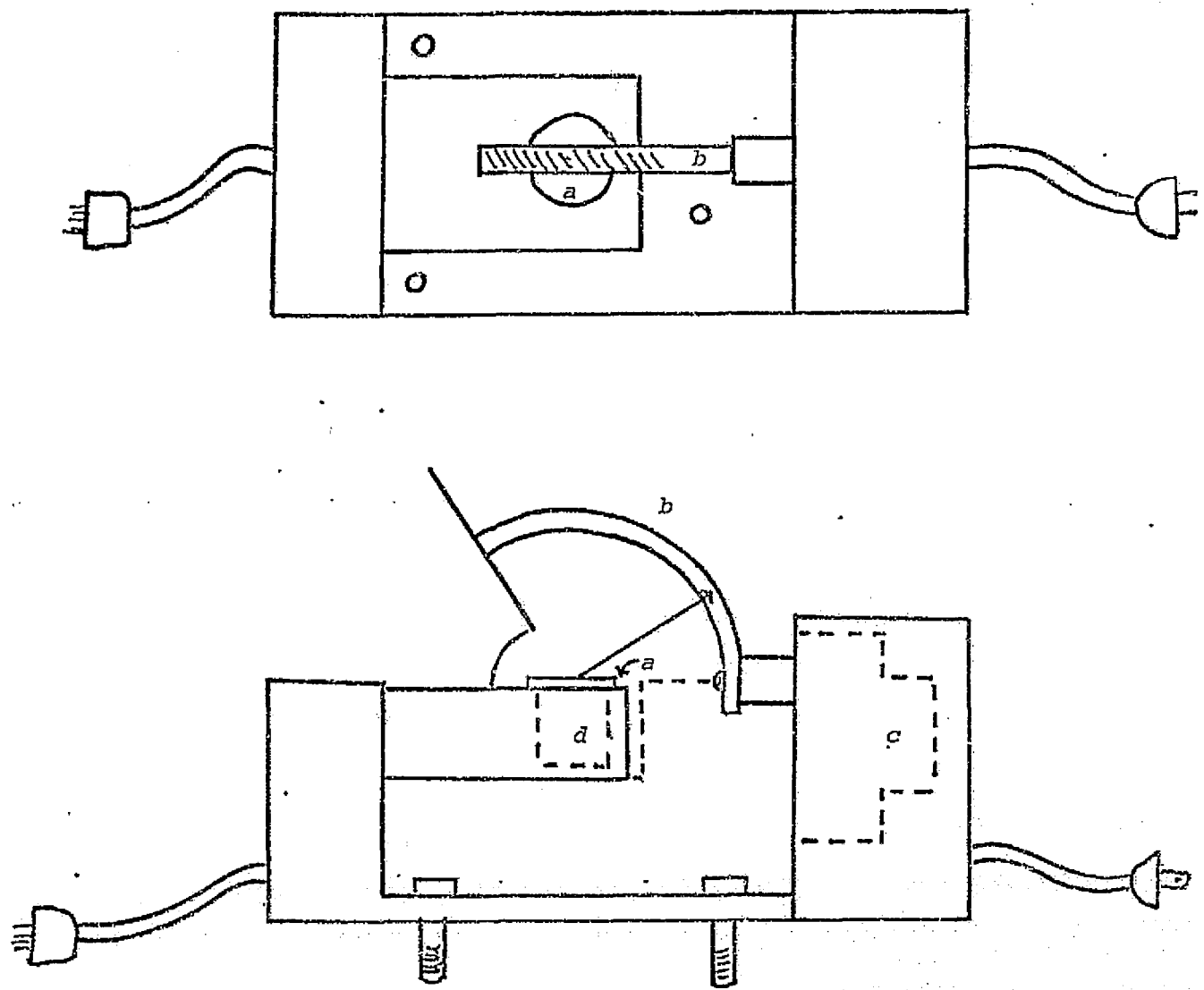
Figure 1. Sketch of the Moving Bar Occulting Radiometer (MBOR)

  a – Aperture Plate
  b – Shade bar
  c – Motor housing
  d – Detector
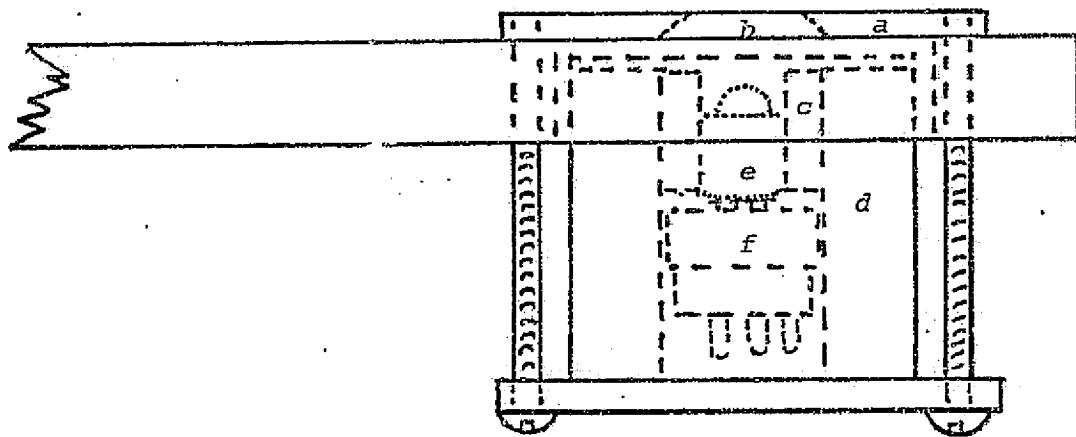
Figure 2. Detector design for the MBOR

a – Aperture plate

b – Diffuser

c – Detector locating sleeve

d – Cell cylinder

e – Detector (TO-5 can)

f – Transistor socket

where d is the aperture diameter and R is the radius of curvature
of the bar. The bar is also cut so its arc length is sufficient
for the maximum solar altitude. A correction factor has been
calculated which takes into account the diffuse radiation lost
to the detector due to the presence of the bar in the 2π stera-
dian solid angle of view. When the bar is out of the detector
field of view, the unit measures the total flux. While the
shadow is over the detector, the instrument is recording the
diffuse insolation.

2.2 Instruments - Electronics

The electronic circuit used to amplify the detector out-
put for Chart Recorder display is shown in Figure 3. This opera-
tional amplifier circuit acts like a current to voltage converter
for the silicon detector operating in a zero bias photovoltaic
mode. The load resistance for the photodiode is near zero due
to the characteristics of the circuit. This guarantees a linear
response for the device in terms of output voltage vs flux level.
The resistor R_3 is used for null adjustment of the amplifier and
the gain is adjustable through R_1 and R_2. A reference current
input is also obtainable from V_{ref} through the precision resistor
R_p to allow for periodic gain stability calibration checks. This
precision reference current source was external to the five indi-
vidual output circuits employed in this research, and was used
as a common source for calibration of the electronics in the field.

-6-
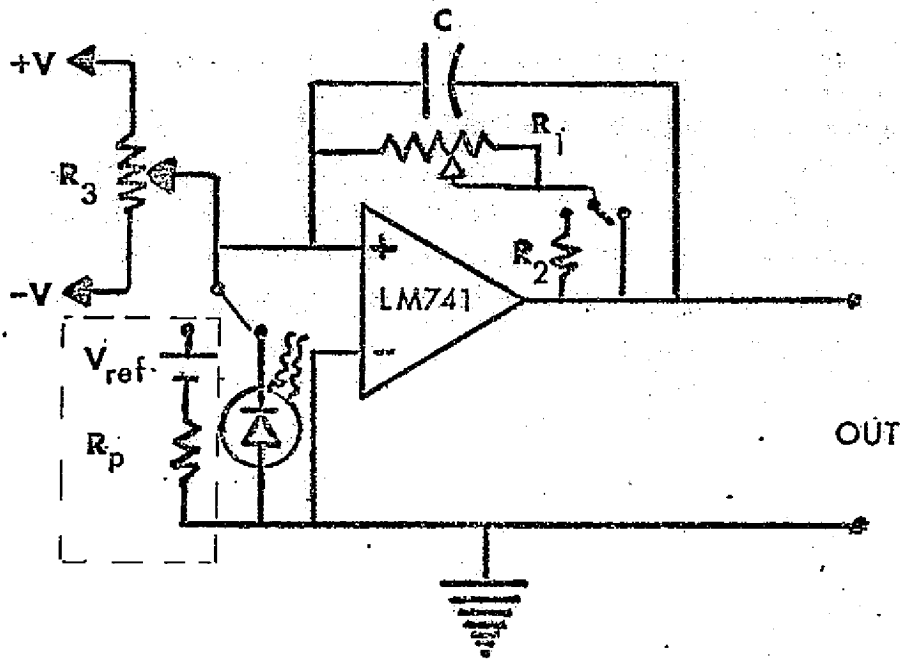
$$C = .0.47 \mu f \qquad R_1 = 2M\Omega \qquad R_2 = 2M\Omega \qquad R_3 = 12M\Omega$$

Figure 3. Schematic diagram of Helio circuit used for the current-to-voltage transducer.

R_1, R_2 feedback resistors ($R_f = R_1 + R_2$ or R_1).

R_3 zero offset adjustment.

V_{ref} reference voltage for circuit gain calibration.

R_p reference precision resistor.

Our experience with these detector-circuit combinations over the past two years has shown them to be extremely reliable and trouble free. In addition, the gain was found to be stable within 1% of full scale and the zero drift was less than 2% per month.

The chart recorders used for the read out of the data are Soltec 10" potentiometric recorders Model 251. The chart speed was 1"/hr to start and 2"/hr in later months. This allowed sufficient reading accuracy for measurements of the flux qualities at 6 min intervals. Each recorder was equipped with an event marker driven by an hourly clock pulse derived from a Bulova interval timer Model TE240. An example of the resulting output record is shown in Figure 4. This analog output shows, at a glance, the total, ϕ_T, the diffuse, ϕ_D, and the direct, ϕ_d, insolation as indicated.

2.3 Calibration and Installation

The instruments were calibrated with respect to an Epply Pyrheliometer by measuring the direct normal solar flux. Each MBOR was tilted perpendicular to the sun, and readings of the total and the diffuse flux were taken. The difference in these numbers was then compared to the reading from the pyrheliometer and the sensitivity calculated. The pyrheliometer was recently calibrated against a group of reference instruments traceable to the National Bureau of Standards. All five MBOR's were adjusted electronically to have the same sensitivity of 7.50 mv/w_{m^2}.
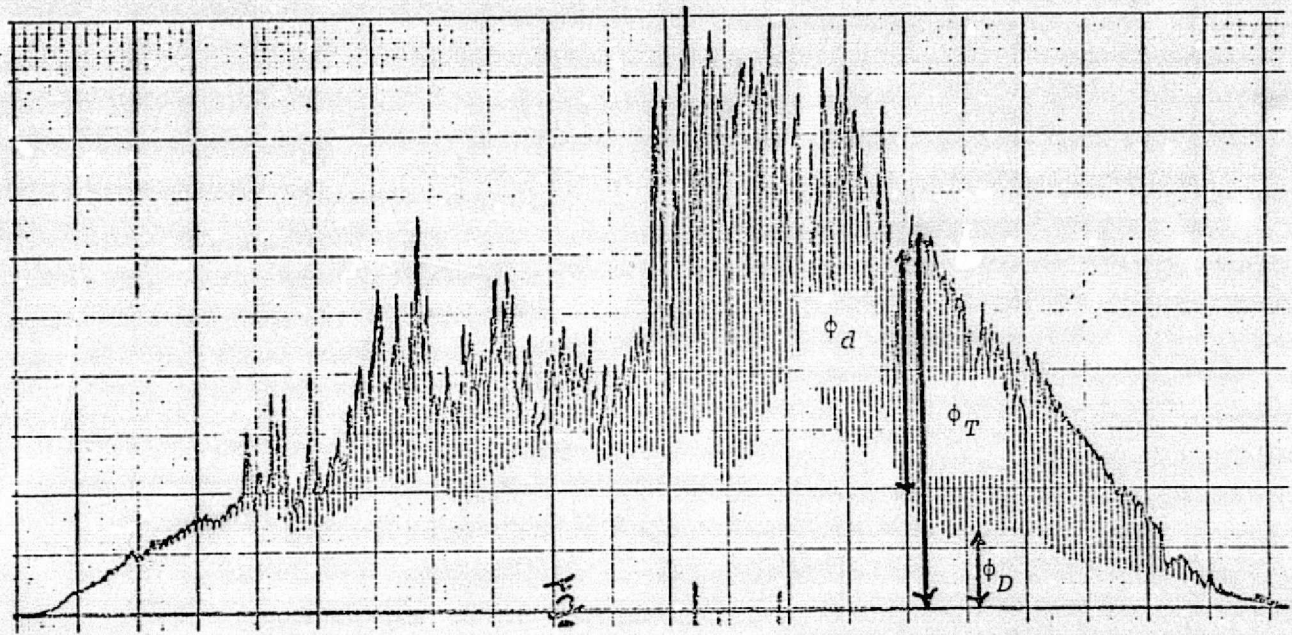
Figure 4. Output of MBOR Instrument

Measurements were also made of the minimum resolvable time for the duration of occultations and the difference in time of occurance of these events. It was found that 0.1 inch is the smallest resolvable occultation due to the width of the chart recorder pen. For a 2"/hr chart speed, this results in a maximum resolvable occultation period of 0.3 minutes. As is discussed later, "events" of this short a duration were difficult to measure because they could not be clearly identified and correlated on all five records. The instruments were located on the grid shown in Figure 5. In this grid, the Helio laboratory was Station 5. The other locations were small convenience markets where electricity and some equipment security were readily available. Relative timing between events (occultations) are used to specify the spatial or velocity profile of clouds over the field. Measurements of the event timing, between Stations 1 and 2 and between Stations 3 and 4, yield two independent measurements of the X component of velocity. Once the velocity is specified, the size of the cloud in the direction of motion can be calculated by examination of the duration of the individual event at each of the five stations. The results of these calculations are values for the representative size, speed, and direction of motion of the clouds.
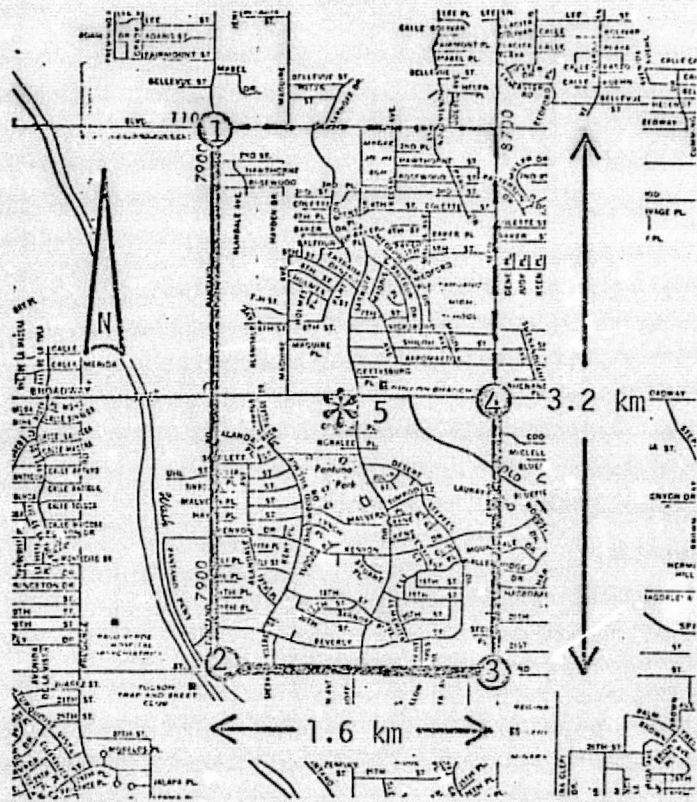
Figure 5. Location of Instruments to measure spatial
distribution of solar insolation. The
asterick represents the Helio Laboratory.

SECTION 3.0 DATA ANALYSIS

The analog insolation data records obtained from each station in the field of detectors are of the form shown by the clear day record in Figure 6 and the cloudy day record in Figure 7. These data are presented in the following consolidations or reduced forms:

      1.) Event analysis employing the five MBOR instruments;

      2.) Calendar day display of the MBOR data for one site;

      3.) Frequency or temporal analysis - Fourier Analysis - and modeling for the MBOR data as read digitally for selected days.

Details of these data presentations are discussed in the following paragraphs.

3.1 Event Analysis

For the purpose of this analysis, an event is defined as any sudden change in the insolation level. On a clear day, the only changes in the insolation are due to angular effects and atmospheric attenuation due to longer path lengths. These changes are gradual and result in a smooth data graph such as shown in Figure 6. On cloudy days, however, there are sharp changes in the insolation as clouds occult the sun or holes in the clouds briefly expose the detector to sunlight. The duration of these events are typically between 1 and 60 minutes,

-12-
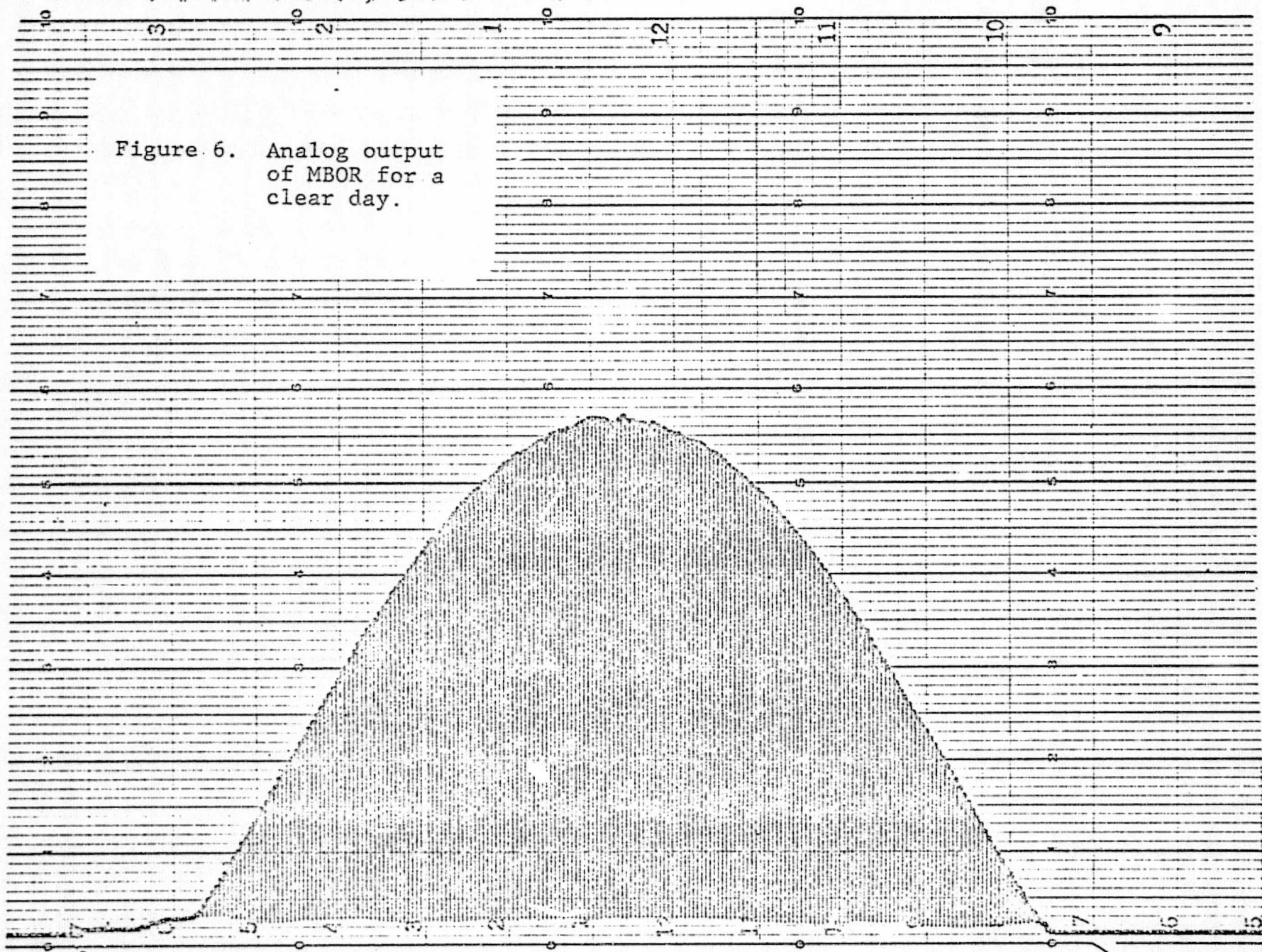
Figure 6. Analog output of MBOR for a clear day.

Figure 7. Analog output of MBOR for a typical partly cloudy day.
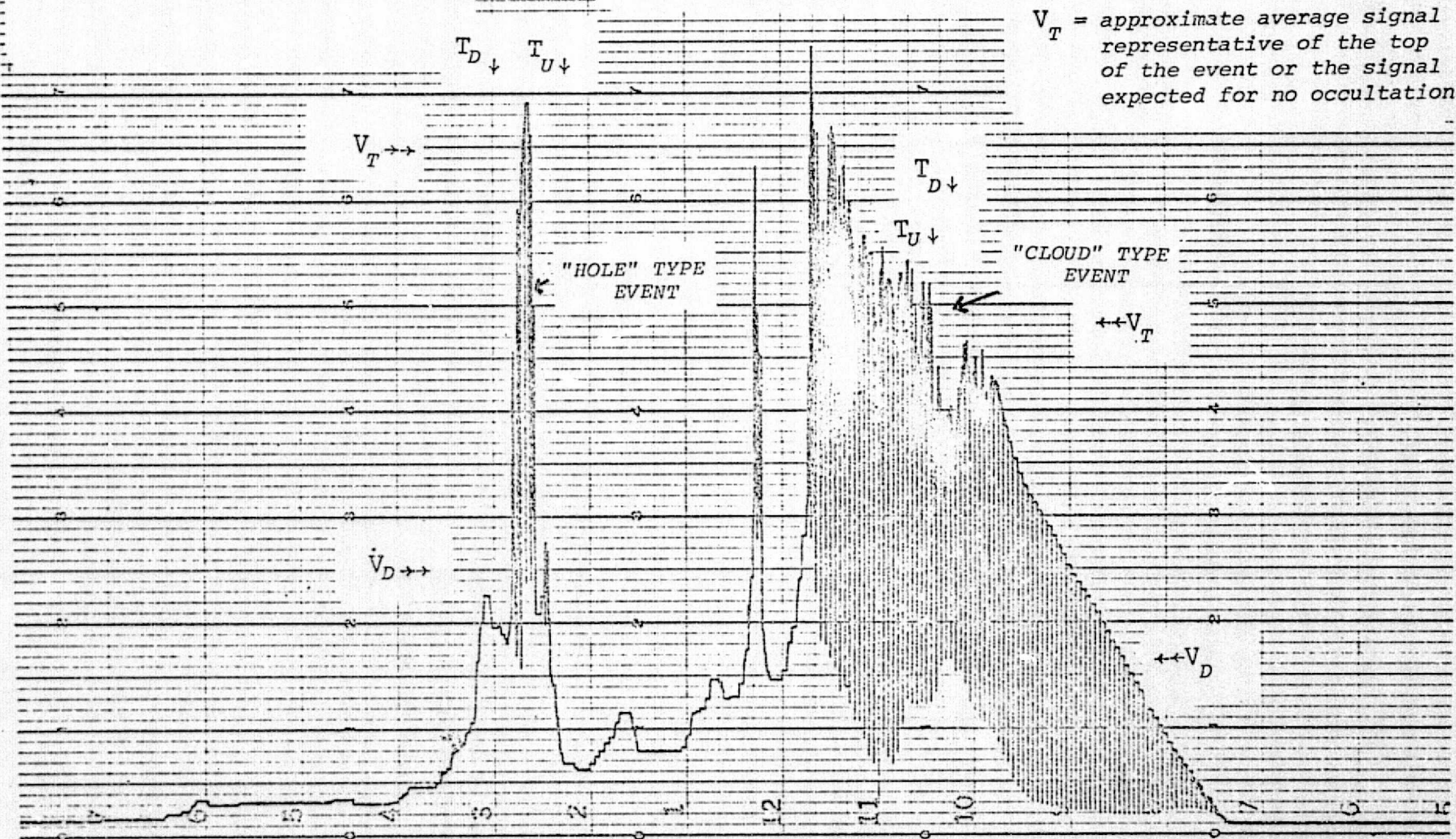
T_U = time reading for any abrupt change from low to high signal for an event.

T_D = time reading for any abrupt change from high to low for an event.

V_D = approx. signal representative of the "bottom" of the event or the resulting solar light intensity during the occultation.

V_T = approximate average signal representative of the top of the event or the signal expected for no occultation.

"HOLE" TYPE EVENT

"CLOUD" TYPE EVENT

-14-

and they can occur frequently and rapidly throughout the day.
The duration of each event and the velocity with which the edge
of the cloud or hole traverses the large collector field are im-
portant considerations for the design of solar power plants.

Each individual detector in the field used in this study
can yield the mean duration of the event and, therefore, the
duration of the loss of input to a part of the collector field.
Comparison of the events between stations can yield the vector
velocity of motion of the cloud across the field. To evaluate
these quantities for selected cloudy days, we measured the event
parameters shown in Figure 7. The quantities T_D and T_U are the
times for the down transition and the up transition for the event
respectively. From these numbers a mean difference or shift in
the time of occultation between adjacent stations is calculated.
These differences, shown schematically in Figure 8, are used to
specify the velocity and direction of motion of the occulting
cloud as shown in Figure 9. Both types of events, "hole" and
"cloud", are represented in Figure 7. The two voltages, V_T and
V_B, shown were also recorded for internal use. If the difference
between these levels is not a large fraction of the total, then
the event is probably uninteresting for anlysis because it would
not be representative of a significant loss in input energy to the
collector system. Therefore, we put a limit on the depth of the
occultation or the height of the peak such that $(V_T - V_B)/V_T > 0.2$.
This threshold value will preclude consideration of the small

Figure 8.   Schematic for the measurement of the time shift for a single event at two stations.

———— Station 1 $\Delta t_{12} = \dfrac{\Delta t_D + \Delta t_U}{2}$

------- Station 2 W = Duration
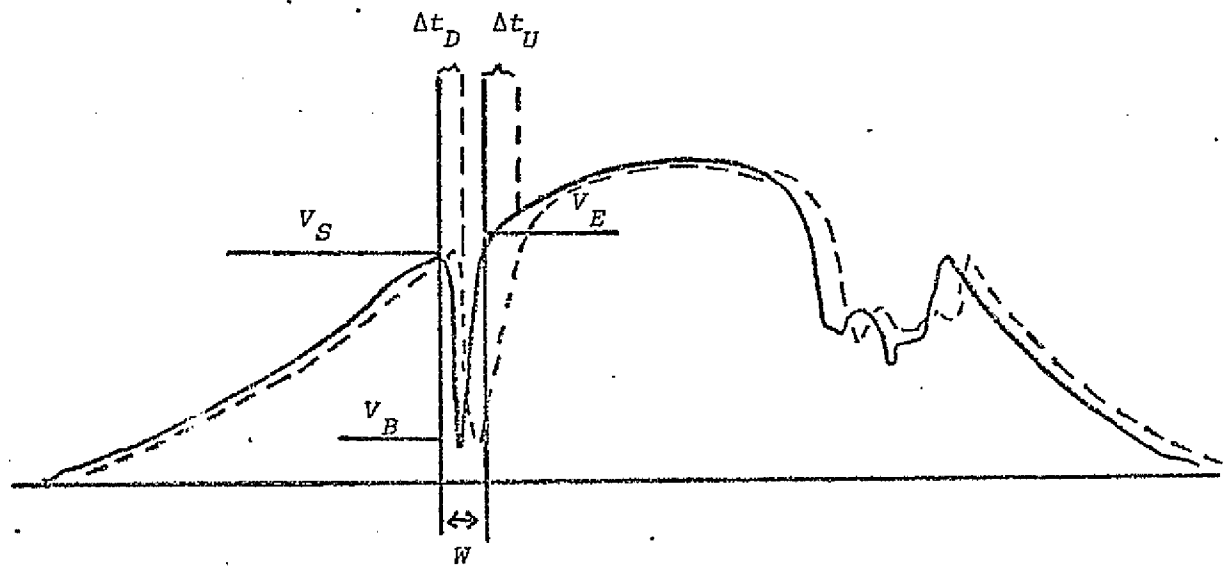
Δt_D = Time shift for the start of the occultation.

Δt_U = Time shift for the end of the occultation.

V_S, V_E, V_B are the signal voltages at the start, the end and the bottom of the event respectively.

Figure 9. Schematic and modeling for the velocity calculations for the field of 5 detectors.
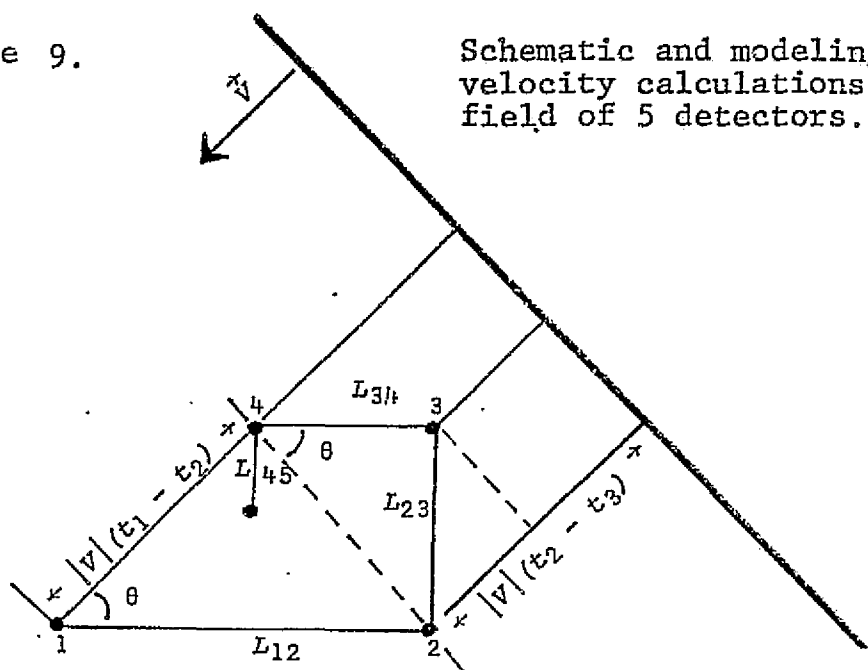
$$\cos\theta = \frac{|v|\,(t_1 - t_2)}{L_{12}} \qquad\qquad \sin\theta = \frac{|v|\,(t_2 - t_3)}{L_{23}}$$

$$\Rightarrow\quad 1 = \frac{|v|^2(t_1 - t_2)^2}{(L_{12})^2} + \frac{|v|^2(t_2 - t_3)^2}{(L_{23})^2}$$

$$|v| = \frac{L_{12}\,L_{23}}{\left[L_{23}^{\,2}(\Delta t_{12})^2 + L_{12}^{\,2}(\Delta t_{23})^2\right]^{1/2}} = \frac{1}{\left[\tfrac{1}{4}(\Delta t_{12})^2 + (\Delta t_{23})^2\right]^{1/2}}$$

$$\theta = \tan^{-1}\left[\frac{L_{12}\;\Delta t_{23}}{L_{23}\;\Delta t_{12}}\right] = \tan^{-1} 2\left(\frac{\Delta t_{23}}{\Delta t_{12}}\right)$$

Similarily

$$|v| = \frac{L_{34}\,L_{45}}{\left[L_{45}^{\,2}(\Delta t_{34})^2 + L_{34}^{\,2}(\Delta t_{45})^2\right]^{1/2}} = \frac{1}{\left[(\Delta t_{43})^2 + 4(\Delta t_{45})^2\right]^{1/2}}$$

$$\theta = \tan^{-1}\left[\frac{L_{34}}{L_{45}}\;\frac{\Delta t_{45}}{\Delta t_{34}}\right] = \tan^{-1} 2\left(\frac{\Delta t_{45}}{\Delta t_{34}}\right)$$

V = Velocity of the Cloud.   *θ = The angle of Motion.*

The L_{ij}'s are the distances between stations along the X & Y direction.

The Δt_{ij}'s are as shown in Figure 4.

-17-

variations in insolation such as characterized by the top of the relatively smooth portion of the data in Figure 7 around 11:00. The angle, θ, will be converted to compass direction according to the schedule in Table 1.

The velocity vector obtained is an approximation to the actual direction of motion due to the possible odd shape of any one cloud. As an example of the reason for this approximation, consider the hypothetical cloud shown in Figure 10. Because the edge of the cloud is tilted to the direction of motion, there is an apparent velocity vector normal to the edge, V_f. This component combines with the actual velocity of motion V_m to form what we see as the velocity, V_r. The magnitude of the difference between V_r and V_m depends greatly on the shape of the particular cloud observed, and although probably small, is not easily evaluated. Therefore, the velocities quoted in this report will be approximate, but still very valuable in power plant design.

The event duration can be combined with the velocity data to obtain representative cloud size data in the form

$$ S = \frac{1}{5} \sum_{i=1}^{5} \frac{T_{U,i} - T_{D,i}}{V} $$

where $V = (V_x^2 + V_y^2)^{\frac{1}{2}}$. These cloud "dimensions" are representative of the extent of the cloud in the direction of motion only. This is the dimension of principal interest for loss of insolation

Table 1.　Table for assignment of compass calculations from the angle of motion determined in Fig. 5.

| Δt_{12} or Δt_{34}	Δt_{23} or Δt_{45}	$=> \phi =$ Compass Direction
+	+	$\phi = \theta$
+	−	$\phi = 180^\circ - \theta$
−	−	$\phi = 180^\circ + \theta$
−	+	$\phi = 360^\circ - \theta$
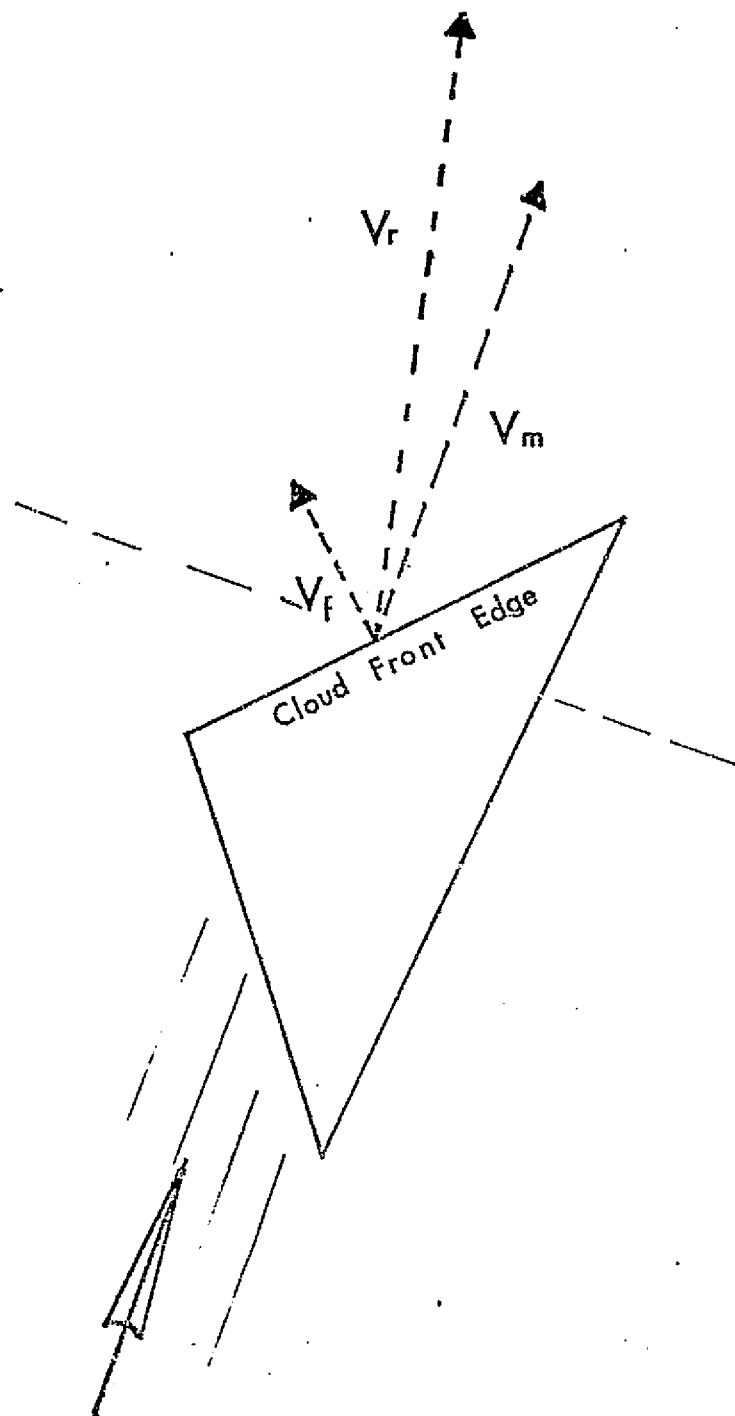
Figure 10. An example of the components of the measured velocity (V_r) due to the actual motion of the cloud (V_m) and due to the shape of the leading edge of the cloud (V_f).

input considerations. The results of these data analyses are presented below.

3.2 Limitations on the Data

Because of the vagarious nature of the weather and cloud formation, the analyses used here are necessarily limited and approximate. In spite of the complexity of the microclimate modeled, we are able to make significant conclusions based on what we feel is a good reliability figure for the data. During the period of observation, we were able to interpret 225 "events" common to at least three stations in the field and subject to the restrictions discussed above. Of these, 134 events did not have usable data from all five stations, and could not be used to calculate the two independent values of velocity. One of the principal reasons for the loss of comparable data was the late speed change in the home base chart recorder. This recorder was maintained for a longer period of time at the 1" per hour chart speed convenient to the calendar data display presented in a later section of the report. This loss of Station 5 data eliminated 32 events from the comparative data. Ninety-three events yielded measurements for all five stations so that the two independent velocities could be calculated. Of these 93 calculations, 62 events yielded agreement in the calculations of both the velocity magnitude and the direction of motion. For the purposes of this analysis, the difference assumed as

limits on the "agreement" of any two values are 50% for velocity, and 45° for direction. In most cases, the angle values resulting for the correlated data are in agreement within 20°, which is excellent.

The 102 remaining events, unusable for the two independent velocity measurements, suffered from various difficulties. About 40% of the events were typified by very fast fluctuations in the insolation which resulted in difficulty identifying the event at corresponding stations. Another 40% of the events were generally well defined, but were missing at one of the stations due to shape, size, or position of the cloud over the field. Another 10% of the event losses were due to paper drive problems. Another 5% were lost due to problems with the electronics caused by electrical storms, and the rest were due to loss of event timing and alignment clock marks due to power outages.

The most common reason for disagreement between the two vector velocity calculations in the 93 fully represented events was sign errors in the event timing. The events which result in these sign errors do not appear to be correlated in cloud size (event duration). They also do not correlate with days which presented difficult alignment or event identification. The most likely cause of these errors is the random nonsymmetric shapes or peculiar angles of the leading and trailing edges with respect to the direction of motion. Of the 93 events, 62 events or 67% show correlated vector velocities. It is our belief that

this level of spatial correlation in the data is excellent considering the complexity of the atmospheric effects involved in cloud motion and the simplicity of the mathematical model assumed for the calculations. In the following section, the results of these calculations with the correlated data are presented.

3.3 Reduced Data - Velocity, Angle, and Size

3.31 Correlated data

An examination of the correlated data shows the findings regarding the local microclimate cloud patterns. These results are also compared with information available from the National Weather Service and the Institute of Atmospheric Physics at the University of Arizona.

The correlated data shown in Figures 11-13 resulted in most probable cloud speeds between 12.8 and 16 km/hr (8 and 10 mph), a most probable direction of motion to the North-West or South-East, and a most probable size around 1.6 km (1 mile). Data published by the National Weather Service for summer Tucson weather, list average observed ground wind speeds during the months of June-August as approximately 8 mph. If we assume the upper level wind speeds are of the same order of magnitude, then we find excellent agreement for our data. Regarding the direction of motion of the clouds, it is a long recognized fact, confirmed by direct communication with the staff of the Institute of Atmospheric Physics, that summer storms in the Tucson Valley tend to move from the SE to the NW. This prevailing pattern is due to
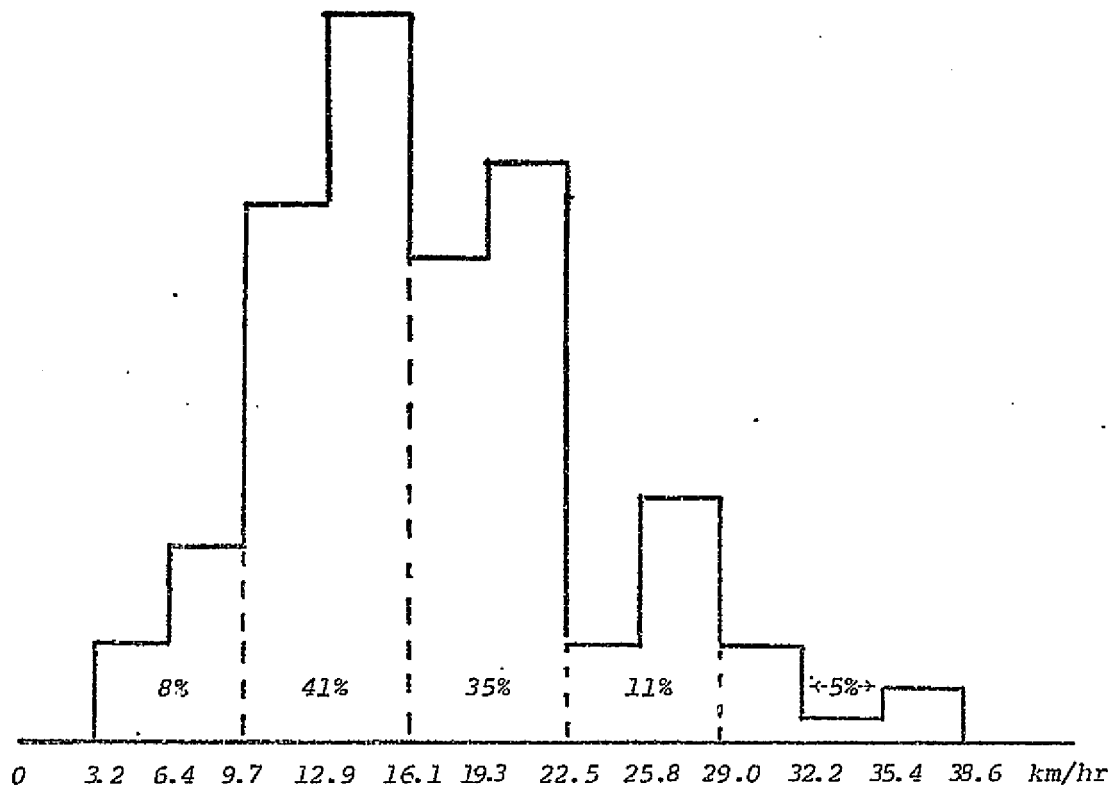
Figure 11.   Velocity distribution determined from
   spatially correlated data.
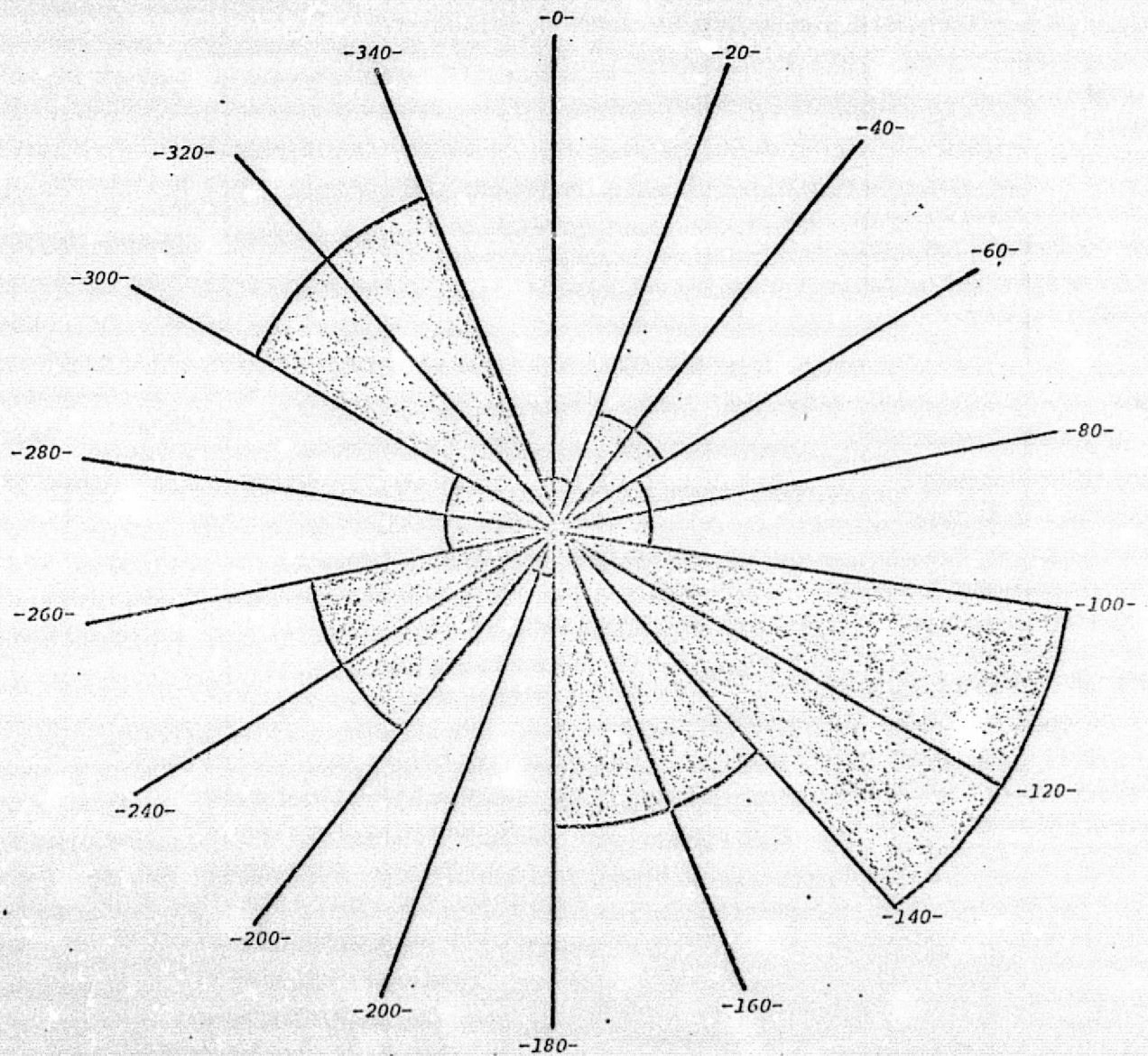
Figure 12. Direction rose for correlated data.
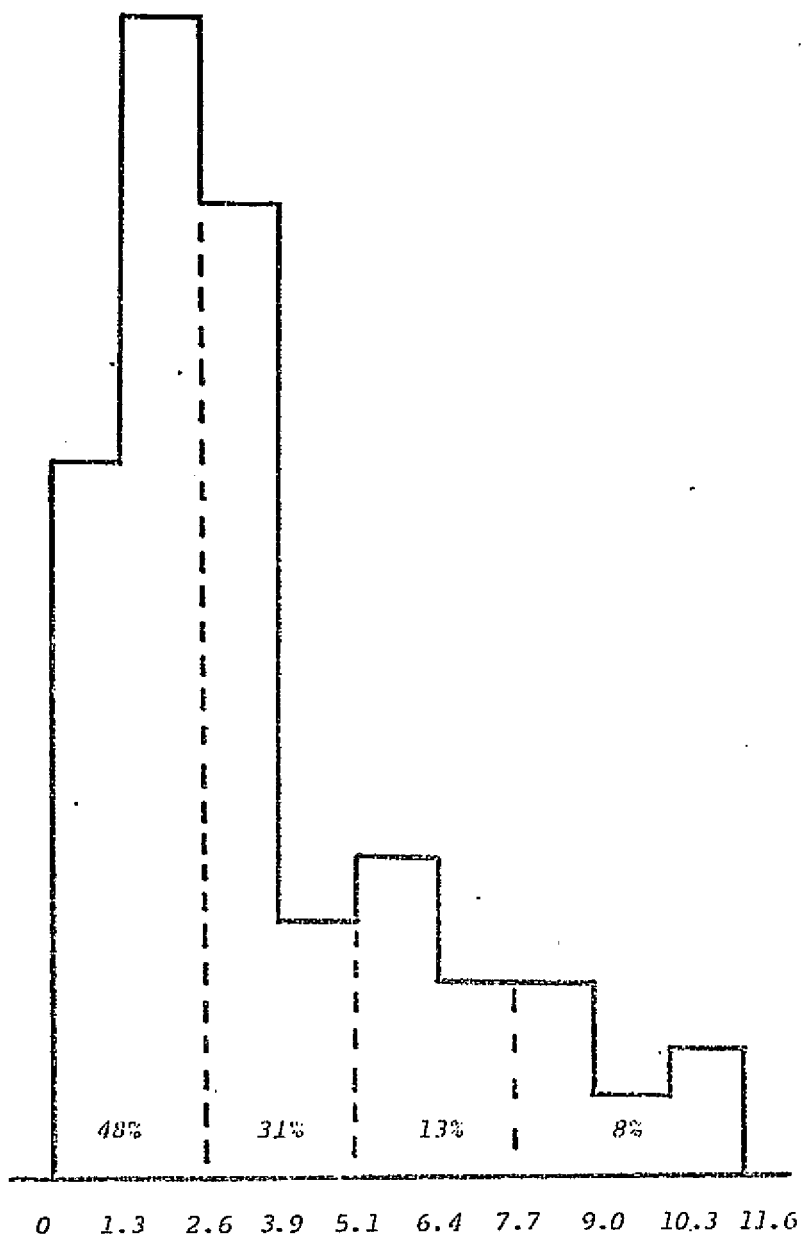
Figure 13. Distribution of calculated cloud sizes, D, (kilometers) from spatially correlated data.

the topological environment around Tucson, and the availability of water vapor from the Gulf of Mexico. The Helio detector field is located in the extreme Northeast corner of the Tucson Valley, within a few miles of the mountains on the East and the North. These mountains, with peaks higher than 2 700 m (9 000 ft), can alter the prevailing storm motions by significant amounts. The data shows a most probable direction of about $130°$ for the observed clouds in excellent agreement with the above pattern.

The cloud size distribution, shown in Figure 14, shows a relatively strong probability for clouds of approximately 1.6 km (1 mile) extent. This result agrees very well with qualitative visual observations of the cloud sizes. There appear to be many clouds of extent less than 0.8 km (0.5 miles), but these do not appear in the data because of the time resolution of the measurement system. Similarily, these observations indicate that individual clouds with sizes greater than 9 km are rare. The specific numbers for velocity, direction and size quoted from the data are only approximate. The variance in the data due to the nature of the events being measured limits the accuracy of the determinations.

3.32 Correlated plus uncorrelated data

To further amplify on the quality of the data as representative of the actual Tucson microclimate, we can examine the complete body of data, including the 134 uncorrelatable events. If these data agree with the correlated data with respect to

cloud speed and direction, we can be confident of the quality of the data for use in the modeling.

The speed and direction distributions for the complete set of data are shown in Figures 14 and 15. The most probable speed is still about 12.8 km/hr (8 mph), but the most probable direction is closer to due West. Considering the latitude in the angle measurements and the possible direction alterations due to mountains, as discussed above, these results agreee with both the correlated data and the prevailing storm patterns in Tucson.

3.4 Power Plant Site Analysis

To analyze the microclimate for a particular power plant location there are several questions which must be answered. If we assume, for our model, that the insolation at the site is occulted by individual clouds on days of partial cloudiness, then the questions that bear the most importance to the operation of a power plant are as listed in Table 2. The answers to these questions can be related to the possible design features of individual components of a collector system, or to the dynamics of the whole system. Let us use the central receiver photo-thermal process as an example. Questions 1-3 are relevant to the initial placement of the system in an area with the least possible insolation interference. Question 4 can give the designer an idea of the extent of dead time to be expected for each individual mirror in the concentrator field for partly

0   3.2   6.4   9.7   12.9 16.1 19.3 22.5 25.8 29.0 32.2 35.4   38.6 41.8   45.0 48.3
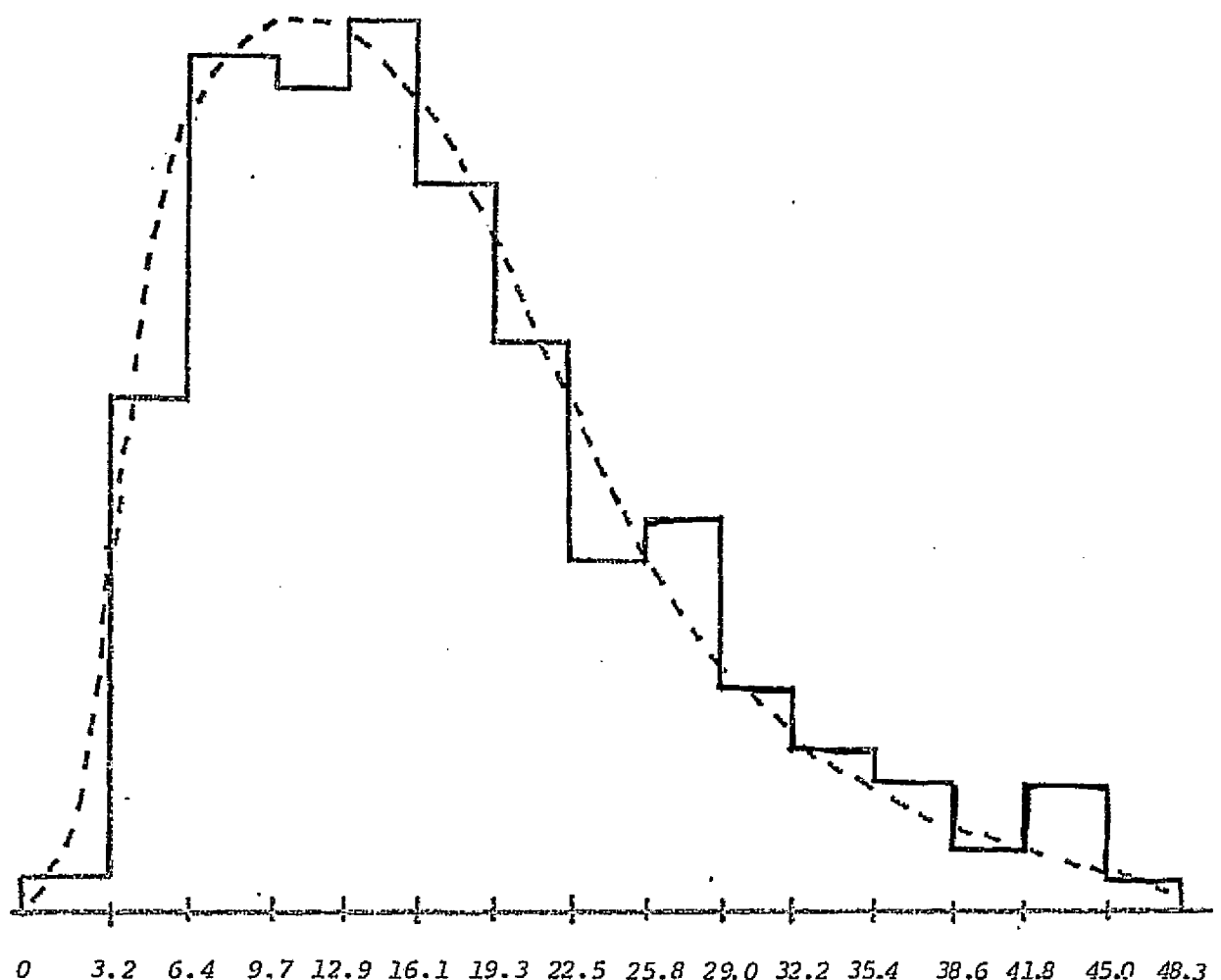
Figure 14.   Velocity (speed) distribution for cloud motion
   over the field using all of the data.
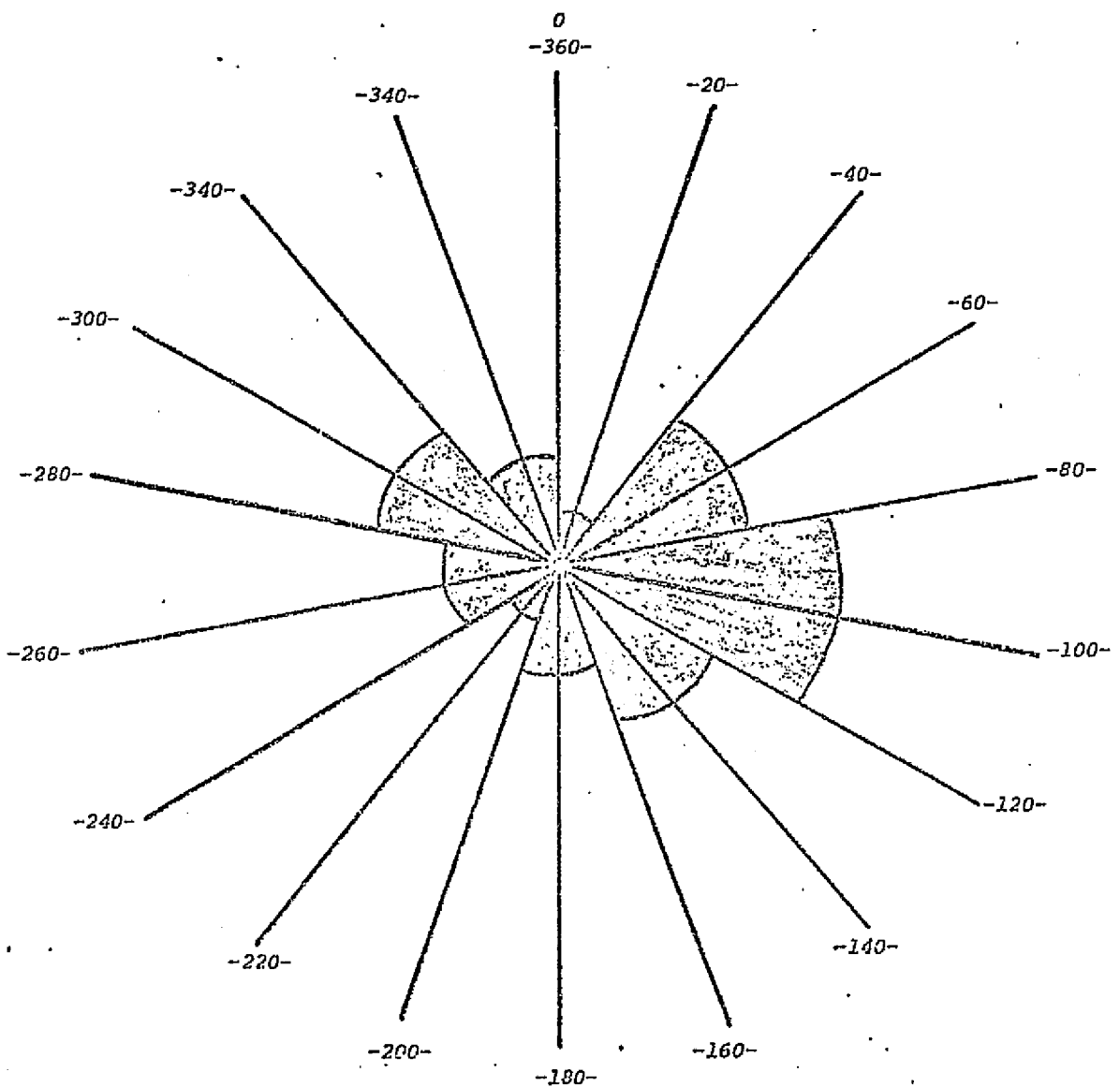
Figure 15.   Direction rose based on all of the data.

Table 2. Microclimatology questions pertinent to power
plant site analyses.

ASSUMPTIONS:	1.)	Each occultation is due to an individual cloud of approximately circular shape.
	2.)	For power plant sizing, the system is assumed to have a 25% overall efficiency for a peak input of 1000 w/m^2, and the field dimension is adjusted to compensate for shading.
QUESTIONS:	1.)	How often do occultations occur.
	2.)	What is the size distribution for individual occulting clouds.
	3.)	Is the temporal distribution for occulting events random or biased.
	4.)	How long will an elemental area in the field be effected.
	5.)	What fraction of the field is affected by any single event.
	6.)	How long will the whole field be effected by any single event.

cloudy days, and questions 5 and 6 relate to the magnitude and duration of differential inputs to the receiver caused by field shading. The answers to these questions are presented below. The data and analysis results amply demonstrate the usefullness of these analyses.

If we examine the data from our field of sensors in terms of the number of partly cloudy days vs the total number of days observed, we find that 29% of all Tucson days have cloud activity leading to possible short duration occultations. For this purpose, a partly cloudy day is assumed to be any day where cloud interference was observed for more than 15%, but less than 85% of the daylight hours. (See the discussion of the calendar day data as listed in Table 4). If we examine the data for statistical bias, we find that there is a slightly greater probability that occultations will occur in the afternoon and evening hours. This is evident from looking at the calendar data at the end of this report. (On these records, the time of day reads from right to left prior to March 18, and left to right thereafter).

The size distribution for the events observed in Tucson was presented in the preceding section. The interpretation of this data with respect to the effects on an elemental area are presented in Fig. 16. The data displayed here is the distribution of the ratio of cloud size to the velocity for each individual event. Therefore, this "dead time" represents the

-32-

$\Delta t\,(hrs)$
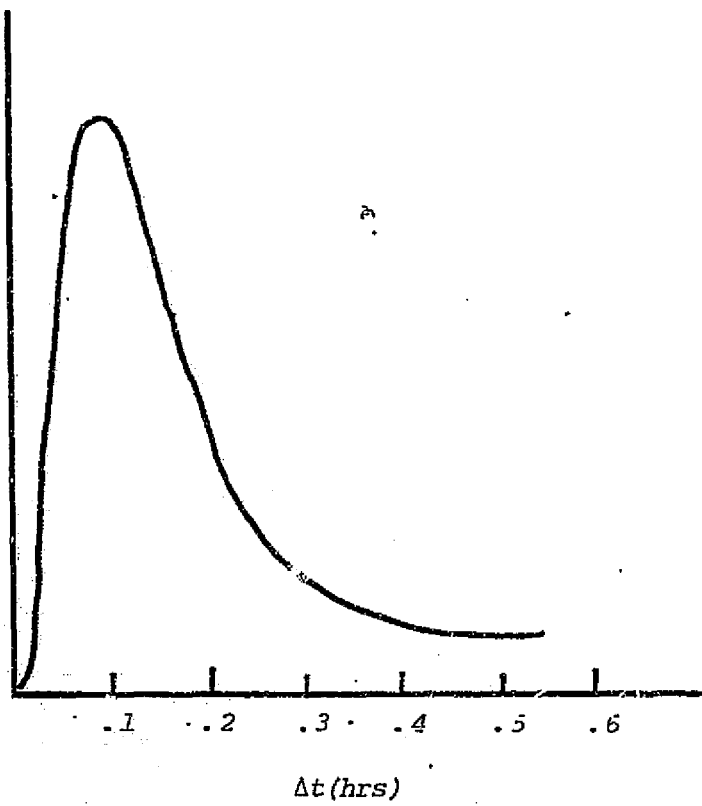
Figure 16. Frequency vs the time any cloud is over an elemental area, ΔA, in the field.

length of time that a particular cloud shades an elemental area of the field or an individual concentrator element. As the data show, the dead time is strongly peaked around 6 minutes. The importance of this information for the central receiver concept, for example, is in the design of the individual concentrator element tracking systems to minimize the loss of mirror alignment after the event clears.

If we examine the fraction of the field area lost during each event, we find the results shown in Fig. 17. For large field systems where the size of the cloud is greater than the mean cloud sizes, the loss of receiver input from the field could cause differential heating problems. For the smaller systems, it is likely that the whole system would lose input due to the cloud, and that the system cooling would be a problem.

The severity of both of these problems would depend on the length of the dead time associated with the event. These results -- the answer to question 6 -- are presented in Fig. 18. As expected, the larger the field, the longer the occultation will cause problems. Data like displayed in Figs. 17 and 18, for any area intended for powerplant siting should be used in optimum size calculations and in the system design considerations.
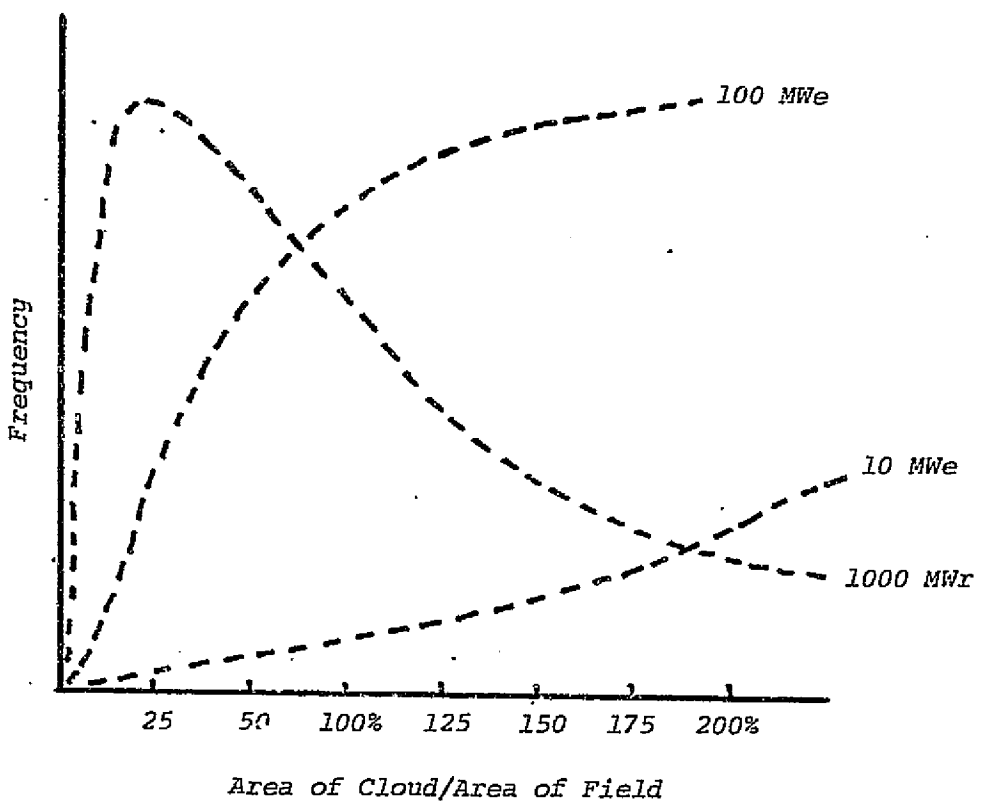
Figure 17. Frequency vs the percentage of the field area that is occulted by an individual cloud.
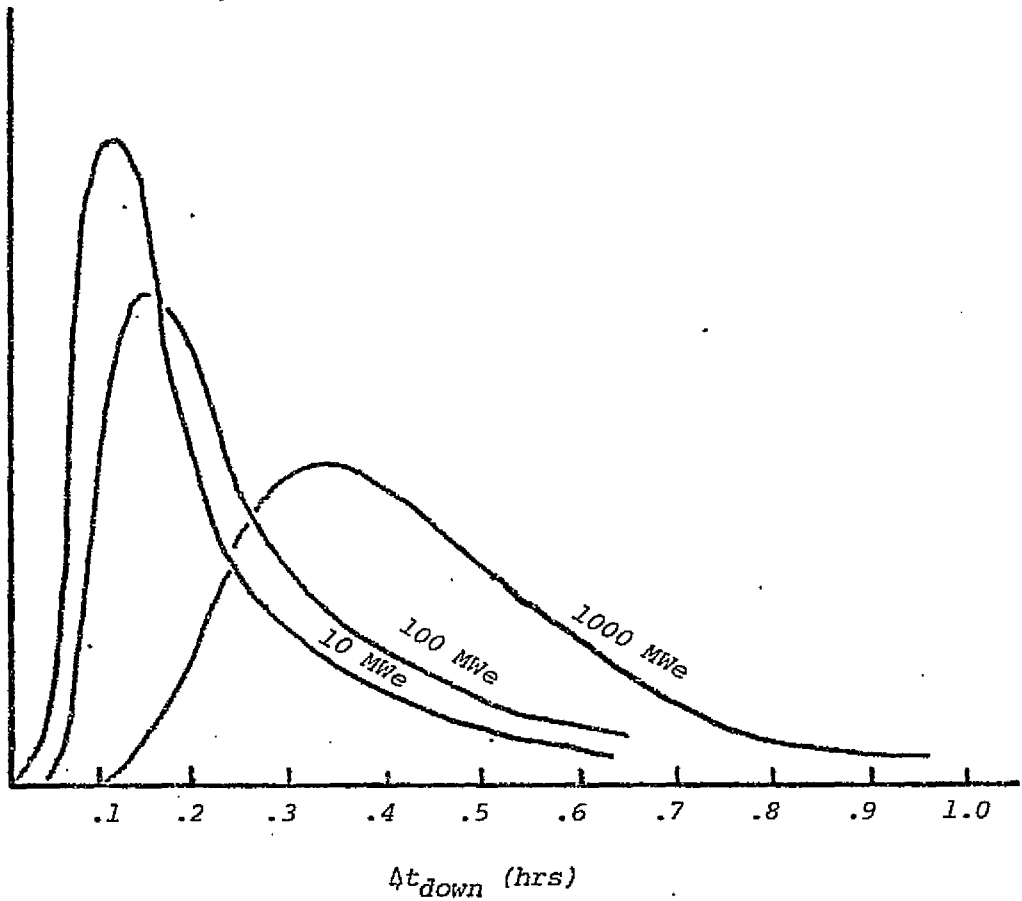
Figure 18.   Frequency vs down time for passage of
             cloud over whole field - largest dimension.

3.5 Fourier Representation

We have found that the solar insolation days for Tucson
fall into one of three categories. Approximately 30-35% of all
days have cloudless skies or very little interference in the
insolation due to clouds. Another 10-15% of all days have heavy
cloudiness or more than 80% sky cover during the daylight hours.
The remainder of the days have moderate cloud activity which may
occur at different·times and alter the solar insolation for 15%
to 75% of the day. The first type of day is relatively straight
forward and simple to explain by the existing insolation models·.
These latter types of insolation days may be easily represented
in terms of the frequency spectrum of the temporal changes in
the insolation. A convenient mathematical model for this fre-
quency representation is the well known Fourier representation
of time dependent functions in the form

$$\phi(t) = \tfrac{1}{2}A_o + \sum_{n}^{\infty} \left(A_n \cos(n\pi t/T) + B_n \sin(n\pi t/T) \right)$$

where

$$A_n = \frac{1}{T} \int_{-\tau}^{\tau} \phi(t) \cos(n\pi t/T) \phi t$$

$$B_n = \frac{1}{T} \int_{-\tau}^{\tau} \phi(t) \cos(n\pi t/T) \phi t.$$

In our previous studies, we have found characteristic
shapes for the data when expressed in this form. A plot of C_n
with respect to $time^{-1}$, results in curves similar to those

shown in Figure 19. These curves are representative of nearly all clear and partly cloudy days observed in Tucson at any particular site and any season of the year. Of course there are variances in the magnitude of the higher frequency components depending on the rapidity of the fluctuations in the insolation.

The Fourier expression may also be extended to show the temporal nature of the cloud motions across a collector field. If we use the velocities calculated from the event analysis, in conjunction with a representative distance across the field, r_{ii}, one can arrive at a model for the temporal-spatial insolation measurements, or local microclimate of the form

$$\phi(t,\vec{r}) \simeq \tfrac{1}{2}A_o + \sum_{n}^{\infty} C_n \cos\frac{n\pi}{T}(t + \frac{r_{ii}}{V} + \gamma_n).$$

In this form, the spatial characteristics of the insolation are represented by an additional phase term.

To evaluate the applicability of this model to our data, we studied the ability to correlate the data between the five individual stations via the addition of various size phase terms to the Fourier representation of a particular day's record. The modeling was considered a success in those cases where the "events" were reproduced from location to location with well preserved widths and depths, but with appropraite shifts in time. The time shifts were deemed excellent if velocities could be calculated and correlated as discussed above.
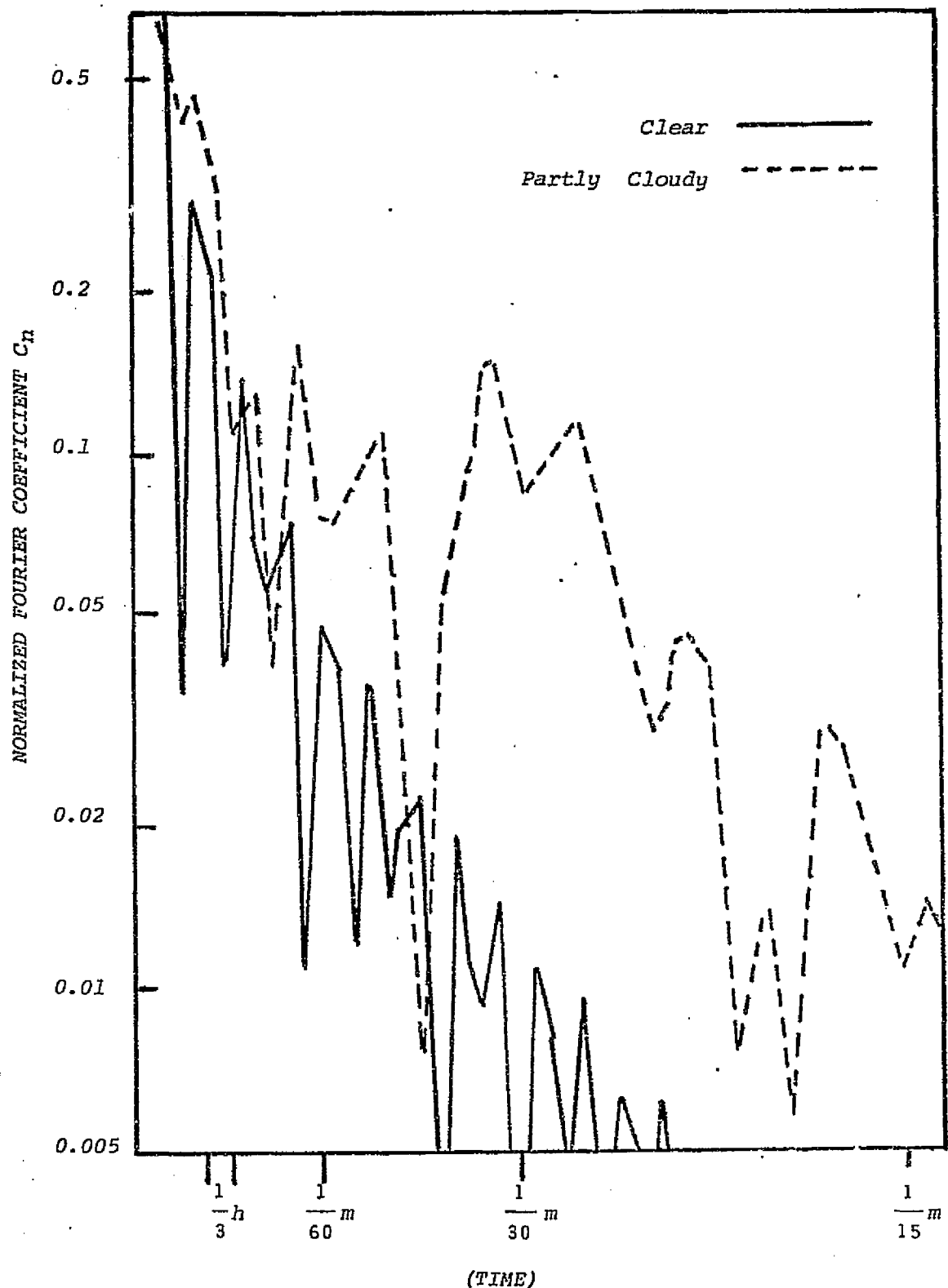
Figure 19. The Fourier Spectra for clear and partly
cloudy days.

The days which showed good Fourier spatial representation,were those days with relatively broad and well-defined occultations; by broad we mean events of duration greater than about 0.1 hr. It was noticed that data records which contained large amounts of high frequency structure, or many events with durations less than 0.1 hr length, were hard to correlate between station locations. These types of days usually were associated with a great deal of variance in both the breadth and depth of individual occultations between the five stations. This variance was not selective with respect to size of the event. The velocity correlations described above were also difficult for such days due to splitting of "events" or fading of an "event" between stations. In particular, occurances such as absence of an "event" on one or more of the records, or "splitting" of a broad event from one station to the next by a spike in the center of the dip, or the combining of two events into one broad dip, were common problems for days with appreciable high frequency activity. These types of phenomena are probably correlatable to particular types of cloud structure. It is most likely that the presence of many short duration events would correspond to light cirrus clouds, cumulus clouds with rough (wispy) eges, or other cloud structures associated with extreme turbulence. The better events are most likely associated with well-defined and well-localized clouds.

The Fourier plus phase representation for each day was judged as good, good-fair, fair-poor, or poor depending on the quality of the fit to all stations. Of the 41 days analyzed, a good fit was found for only 15 days. If the fair to good days are included, the count is increased to 26 days. The fair to good days are those where the fit was applicable for more than half of the identifiable events. The greatest fault was in the reproduction of the widths and depths of the events. The poor days were generally associated with large variences in both width and depth of the events or with missing events on one or more station record. The ability to relatively well account for the five stations, 26 out of 41 times using the phase shift model yields a 63% confidence in the model. We would, therefore, conclude that the technique is applicable to microclimate predictions, but limited in its accuracy.

A good estimate of the phase term can be caluculated by using the most probably magnitude of velocity as detemined from the velocity profile such as shown in Figure 14. If one then references to a particular location in the field, the phase term can be calculated for any other point at a distance $|\vec{r}|$ away.

By examining the Fourier representations of the days, one can type days according to the six classifications shown in Table 3. The applicability of the Fourier-Phase model for each type of day is shown by a "G" for good, a "G-F" for good to fair, or a "P" for poor.

Table 3. Day classifications and the results of Fourier plus
          phase modeling for each.

DAY TYPE NO.	DESCRIPTION	FOURIER + PHASE
1	Nearly clear with well defined occultations and very little high frequency activity. Example: June 29, 1975 - Figure 27	G
2	Nearly clear with well defined occultations and some high frequency activity. Example: February 16, 1975 - Figure 23	G-F
3	30-80% of day contains occultation "events" or activity. Much high frequency activity. No overcoat period. Example: January 9, 1975 - Figure 22	P
4	30-80% of day contains occultation activity. Overcast for part of day. Little high frequency activity. Example: January 7, 1975 - Figure 22	G
5	30-80% of day contains occultation activity. Overcast for part of day. Much high frequency activity. Example: January 27, 1975 - Figure 22	P
6	Overcast day with sharp peaks. Example: March 8, 1975 - Figure 24	F-G

3.6 Calendar Representation

The data obtained from the MBOR instruments can also be displayed in calendar format. This display shows, at a glance, the nature of the solar insolation during the months. The number of clear days, the trends through the weeks, and the types of cloudy days during the month, are all readily obtainable from even a cursory study of the calendar.

Included in this report as Appendix 1, Figures 20-27 are the calendar data for November 1974 through June 1975. After June, the Home Station recorder was shifted to the 2"/hr speed, making the calendar photography impractical. Inspection of these records yields some very interesting information. Let us assume the classification of the days as follows:

Clear - <15% of day's insolation
interruped by clouds;

Partially Cloudy - >15%, but <85%
of day interrupted;

Overcast - >85% of day interrupted.

Application of this scheme to the five months data results in the breakdowns shown in Table 4. The data shows a rather remarkable constancy in the fractions of the type of insolation days observed during the three seasons.

Table 4. Division of Calendar-Day data into three classifications showing similarity of the eight Winter/Spring/Summer months.

NO. DAYS OF DATA	MONTH	NO. OF DAYS O.C.	NO. OF DAYS PARTIAL	NO. OF DAYS CLEAR
30	Nov. 1974	2→7%	11→37%	17→57%
30	Dec. 1974	3→10%	5→17%	22→73%
31	Jan. 1975	3→10%	8→25%	20→65%
26	Feb. 1975	1→4%	8→31%	17→65%
30	Mar. 1975	2→7%	12→40%	16→53%
26	Apr. 1975	5→17%	9→30%	12→40%
31	May 1975	1→3%	10→32%	20→65%
26	Jun. 1975	0→0%	4→13%	22→73%

3.61 Comparisons with NWS data

We may also present the data in Table 4 in graphical
form as shown by the solid lines in Figs. 28 and 29. The data
can then be compared to the pertinent National Weather Service
information for the same months. The two sets of NSW data
which should have close correlation to our "days type" analysis
are the percent of cloud cover, and the percent possible sun-
shine. The observations of percent cloud cover are of a quali-
tative nature because they depend on observational judgements of
individuals regarding the fraction of the sky that contains
clouds. It is our experience that the proximity of mountains
and the "bowl" shape of the Tucson Valley yield many days where
there is significant amount of cloud cover which only minimally
obscures the valley floor. Much of the cloudiness is well
localized over the mountains in these cases. This may be the
reason for the relatively poor agreement in the percentages
displayed in Fig. 28. In this figure, the lower lines are the
percentage of days for each month that correspond to "clear"
skys. Clear skys are defined as days with less than 15% activity
or less than 1 tenth cloud cover. The area between the two lines
represents the partly cloudy percentage given by 15-85% activity
and 1-9 tenths cloud cover.

Of perhaps more significance is the correlation between
the "percent of possible sunshine" and our analog data. The %
sunshine readings are calculated from the ratio of the total

Figure 28.   Percentages of days classifed as clear, partly
             cloudy, or overcast for the months of November
             1974 through June 1975.

90

80

70

60

50

40

30

20

10

N   D   J   F   M   A   M   J

OVERCAST
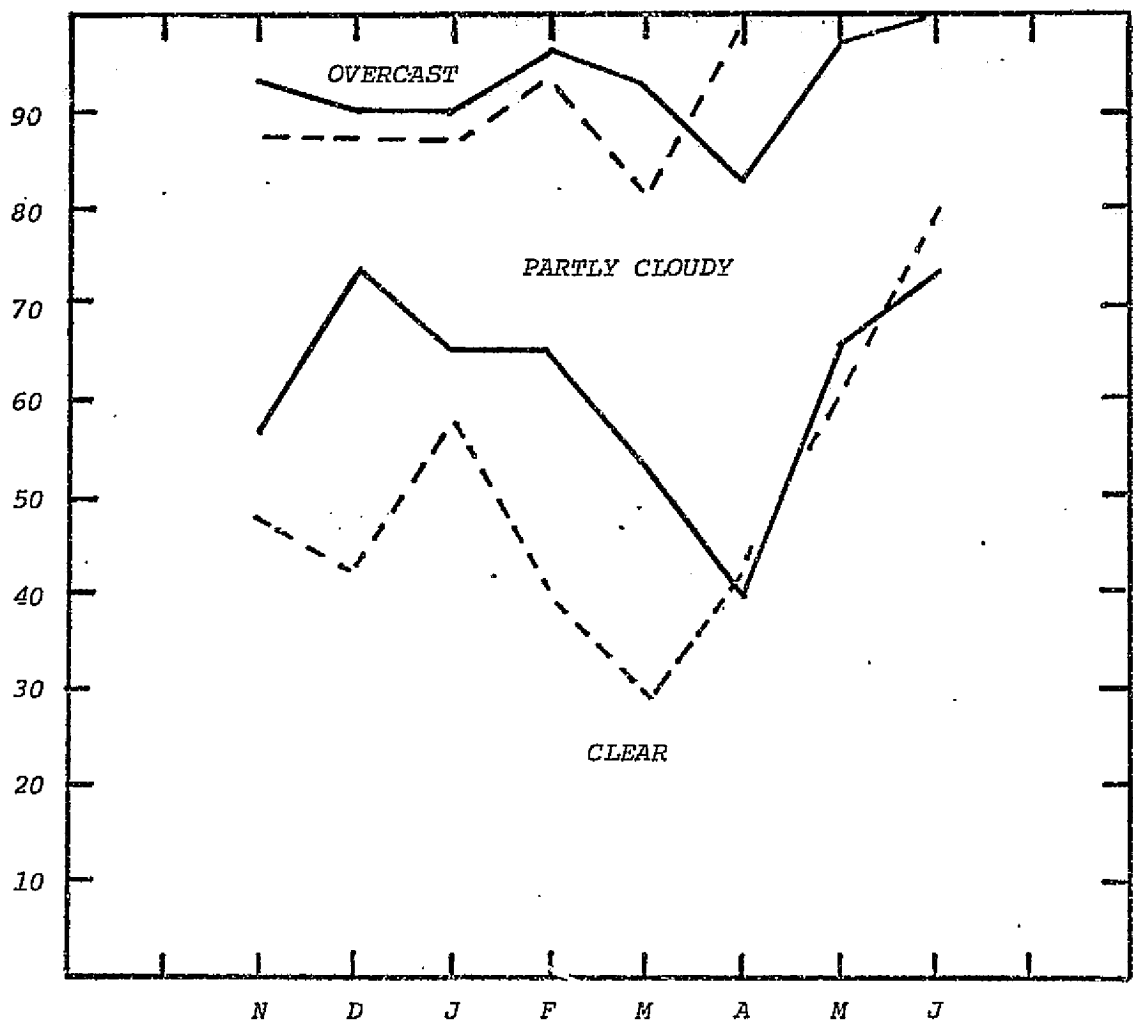
PARTLY CLOUDY

CLEAR

HELIO Data (Solid Line)
    Clear   => <15% Activity
    Partly Cloudy =>   15%< Activity <85%
    Overcast   => >85% Activity

NWS % Possible Sunshine (Dashed Line)
    Clear   => >85%
    Partly Cloudy =>   15<% Sunshine <85%
    Overcast   => <15%

Figure 29.   Percentages of days classified as clear, partly
cloudy, or overcast for the months of November
1974 through June 1975.

number of hours when the direct insolation is greater than zero to the number of hours between sunrise and sunset. There are many times when occulting clouds to not totally obscure the sun, i.e. the direct flux does not go to zero during the occultation. Examples of this are apparent in the calendar records for November in Fig. 20. November 13 and 14 are excellent examples. These difficulties could easily account for the differences shown in Fig. 29. The interesting result of our measurements is that the partial occultations are evident in these records. The % possible sunshine data can be significantly misleading as to the total direct insolation available at a site. It should be emphasized that the device used to record the "possible" sunshine record is merely a switch which turns on or off as the insolation exceeds or drops below a threshhold value. The device is usually adjusted to "turn-on" when the direct flux is just enough to yield a definite shadow for an object.

SECTION 4.0 CONCLUSIONS

The analysis of the data as presented above yields much valuable information for the designer of large scale solar absorber systems. The data obtained from this study can be used to develop the most efficient system configuration and/or controls for any system for any particular site. The micro-climate statistics available from these measurements are a good representation of the insolation dynamics expected for a large field array. This data can be statisically analysed to allow design input of the probability of insolation interference and the dead times expected for individual elements of the field or the field as a whole. These data, in conjunction with the area losses and imbalances due to occultations, are essential to the achievement of a best cost effective design for large solar collector systems.

Comparisons of the Helio data records to the NSW data, results in qualitative correlation. The differences in the two data sources seem to be attributable to the loss of infor-mation content inherent to the methods of measurement employed by the NWS or to the separations of several miles between the NWS station and the Helio network.

SECTION 5.0 <u>RECOMMENDATIONS FOR CONTINUED RESEARCH</u>

The statistical analyses presented here have demonstrated the usefulness of the microclimatological modeling of power plant sites. The data base presented is, however, only minimal, and should be expanded and refined. It is our belief from visual observations that a great deal of the cloud occultations had periods less than the temporal resolution of the system. It is, therefore, recommended that this resolution be improved. This is easily accomplished by increasing the recorder drive speeds to "spread out" the data, and the improvement of the clock timing system used to correlate the five individual records.

In addition, there are other data correlations which may prove very useful. In particular, the use of correlated photography of the occulting clouds and their type may be useful in relating the field temporal statistics to cloud type and cloud cover statistics available from the Weather Service. The data analysis should also be expanded to yield comparative models for both focusing and non-focusing systems in which we may be able to describe the magnitude of the insolation changes at any point in the field, $\Delta\phi(R_{ii})$, in terms of a probability distribution. These distributions could be calculated for both the direct and the total insolation for applications to concentrating or planar systems. This modeling would present data on the fractional loss of input energy and would be useful in specifying the type of system best suited to a

particular site. The continuation of this work is the subject of a proposal presently being drafted.

SECTION 6.0 <u>APPENDICES</u>

APPENDIX 1

Figures 20 through 27:

     Calendar display of the analog data for the months
of November 1974 (Fig. 20), December 1974 (Fig. 21), January
1975 (Fig. 22), February 1975 (Fig. 23), March 1975 (Fig. 24),
April 1975 (Fig. 25), May 1975 (Fig. 26), and June 1975 (Fig. 27).
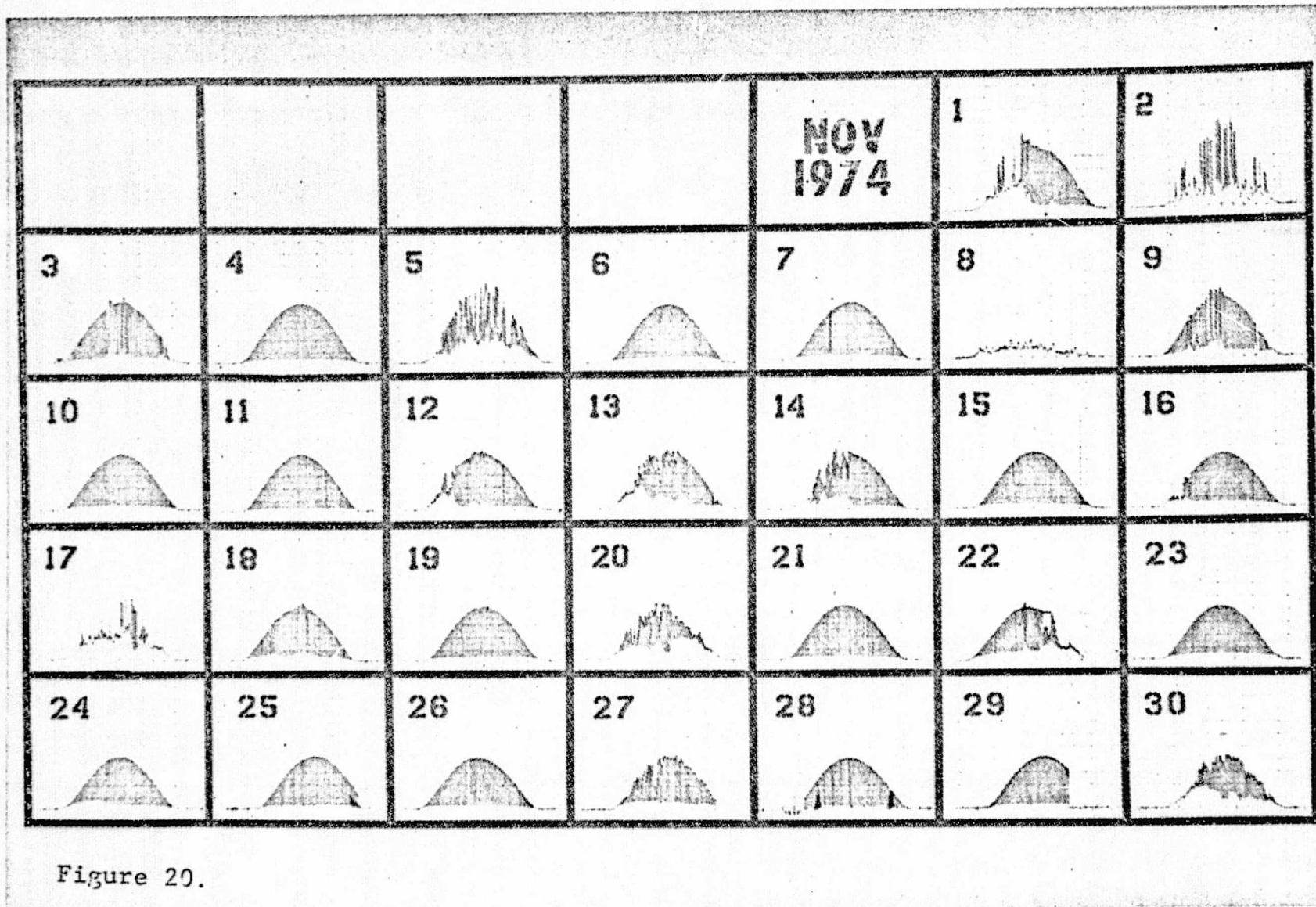
Figure 20.
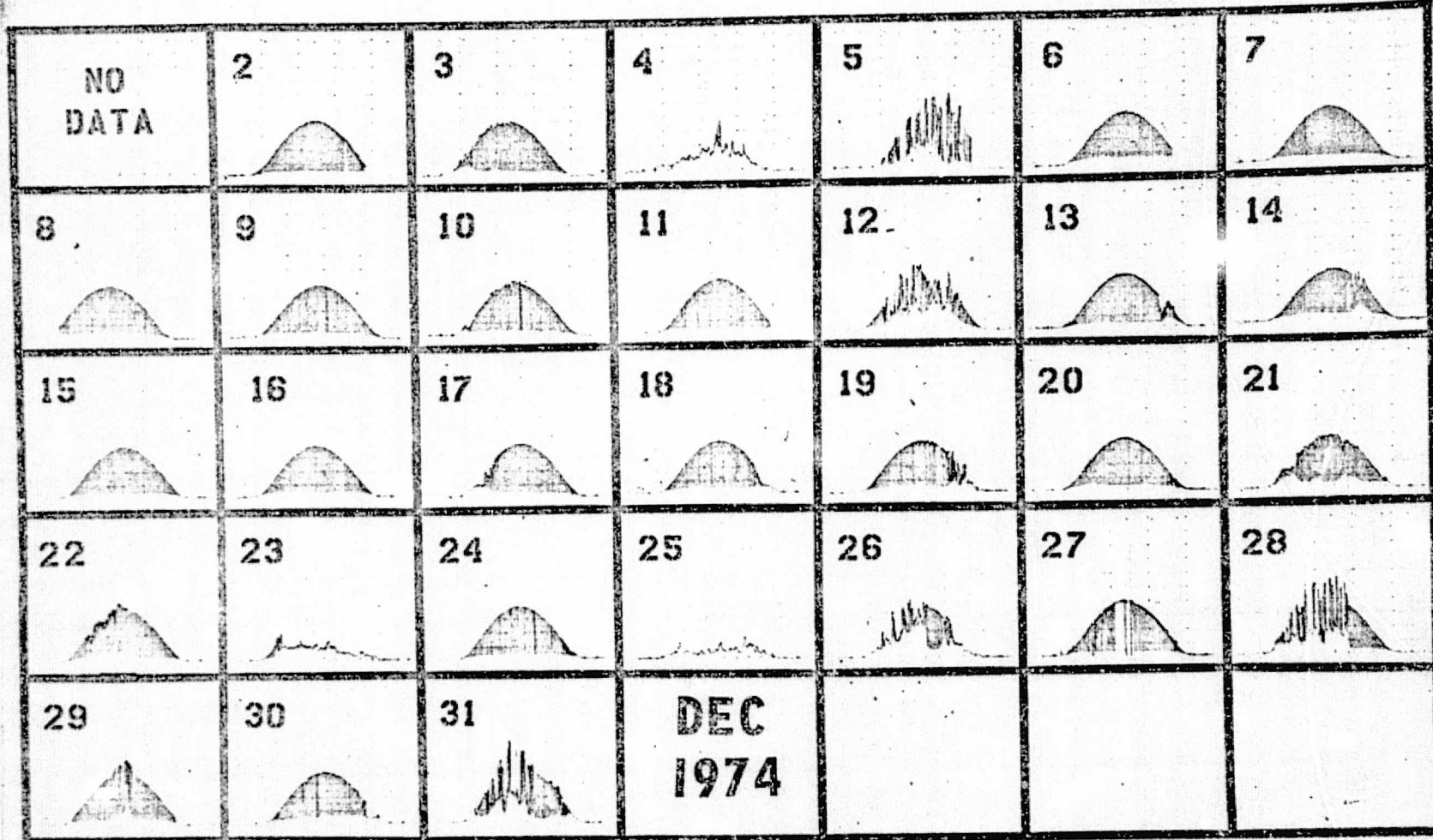
Figure 21.
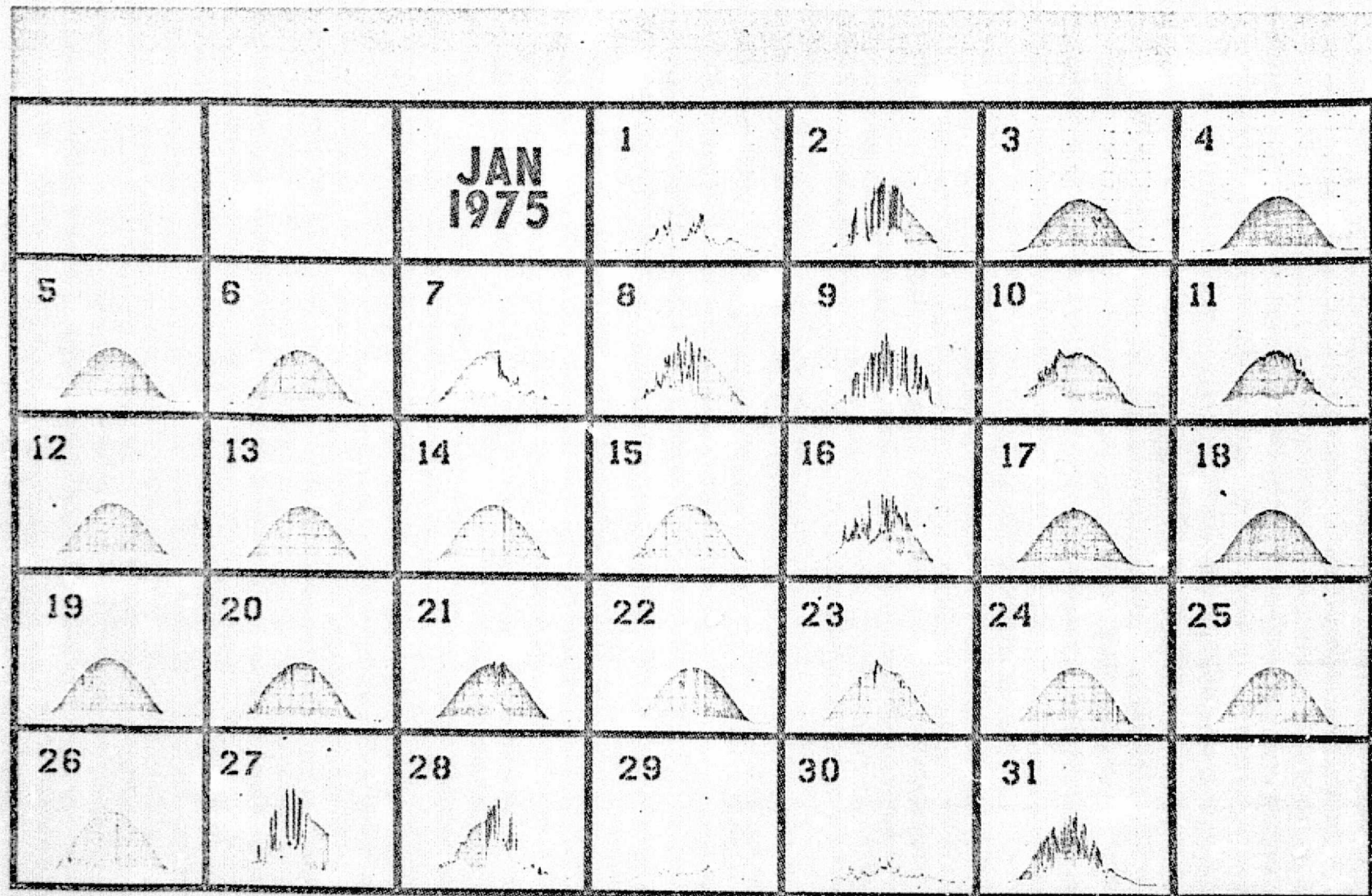
Figure 22.
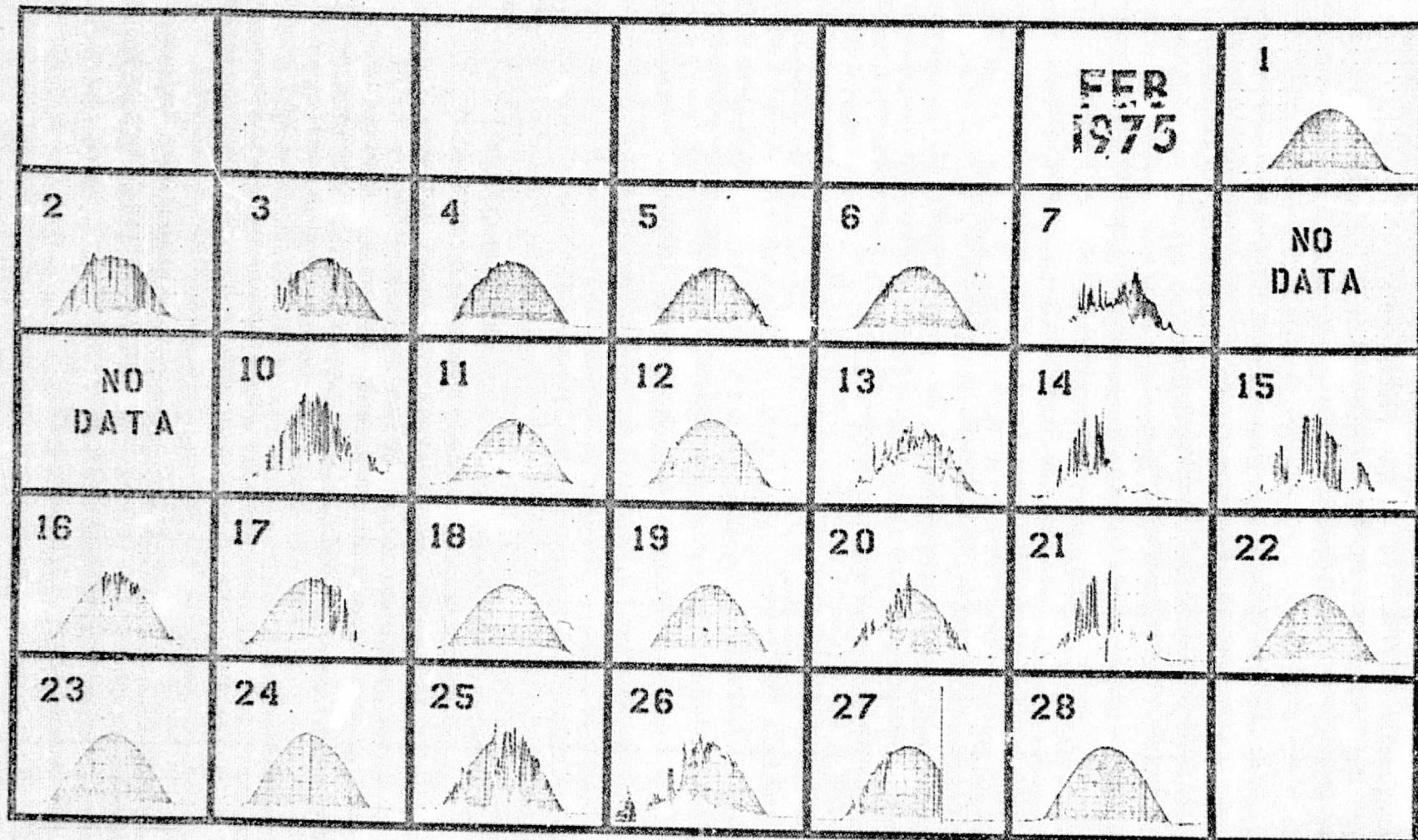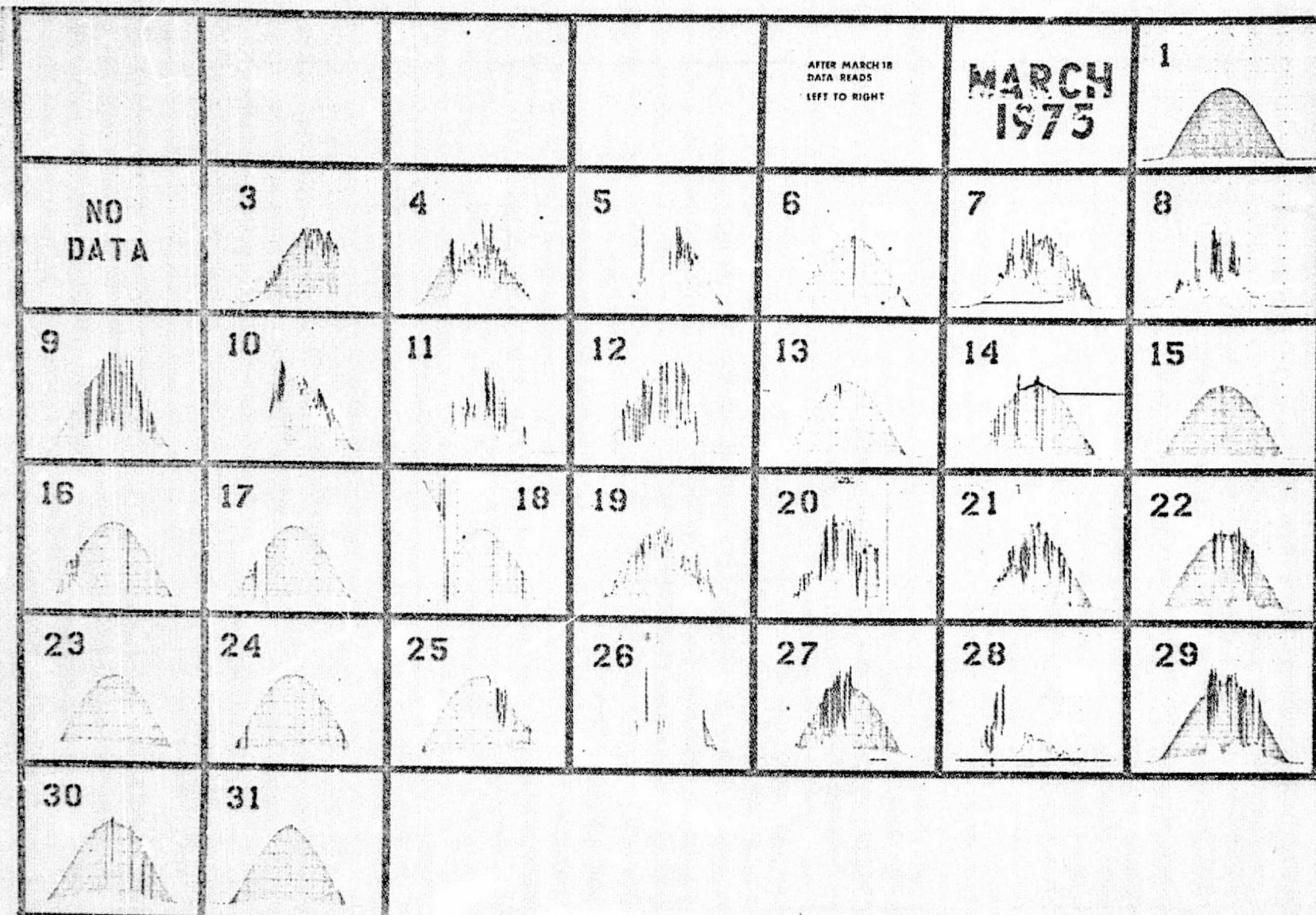
Figure 23.

Figure 24.

Figure 25.

-52-
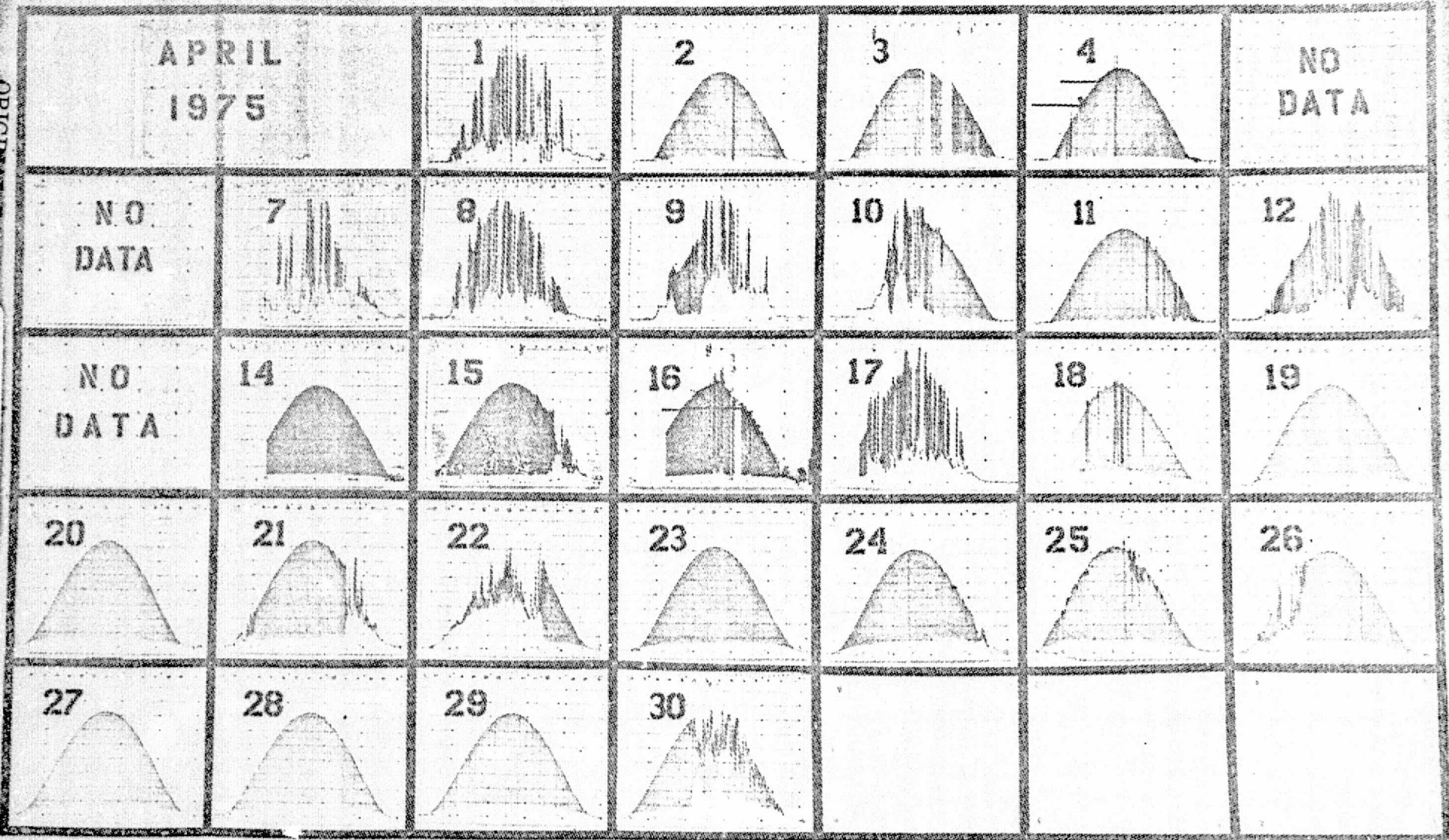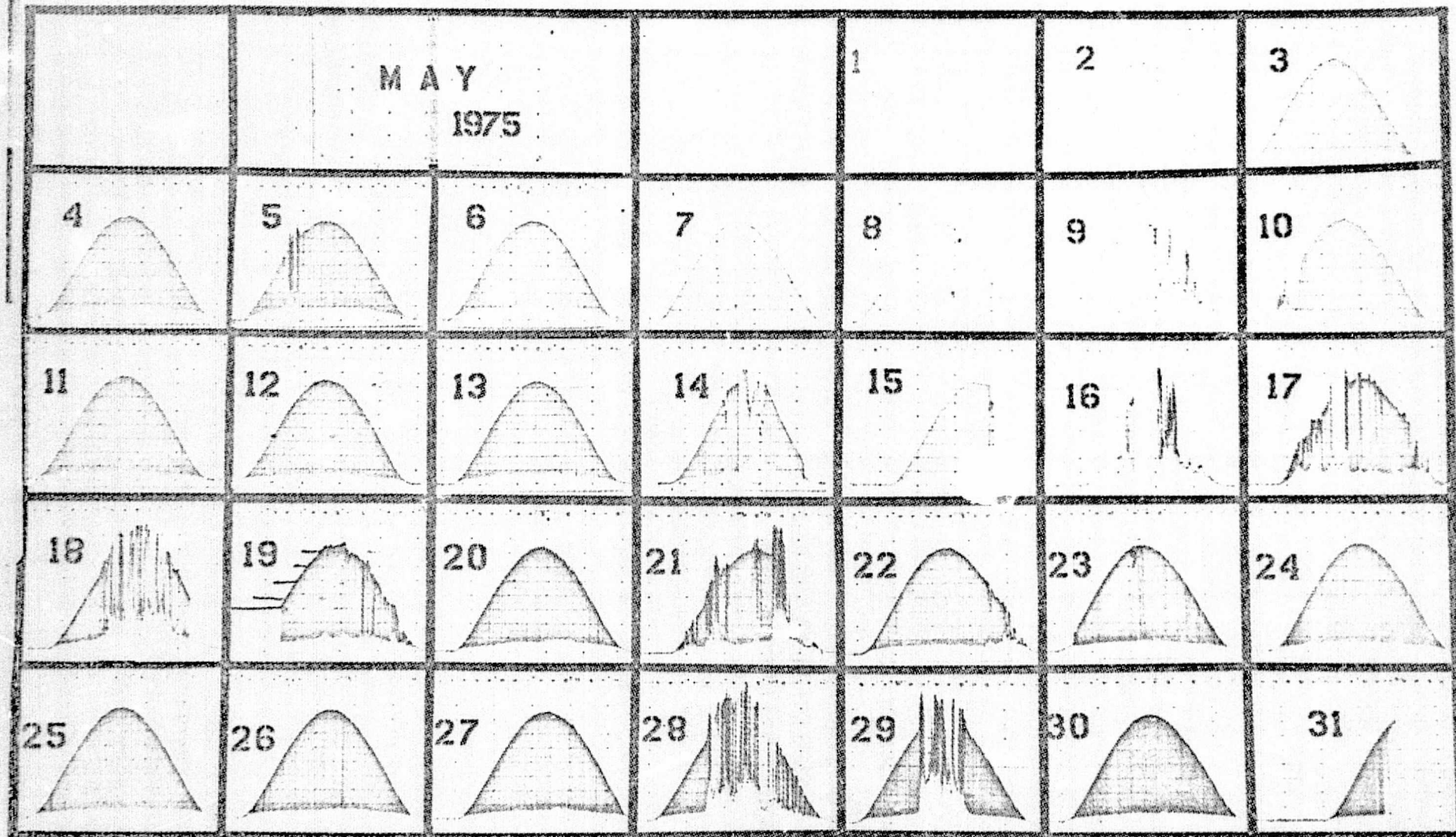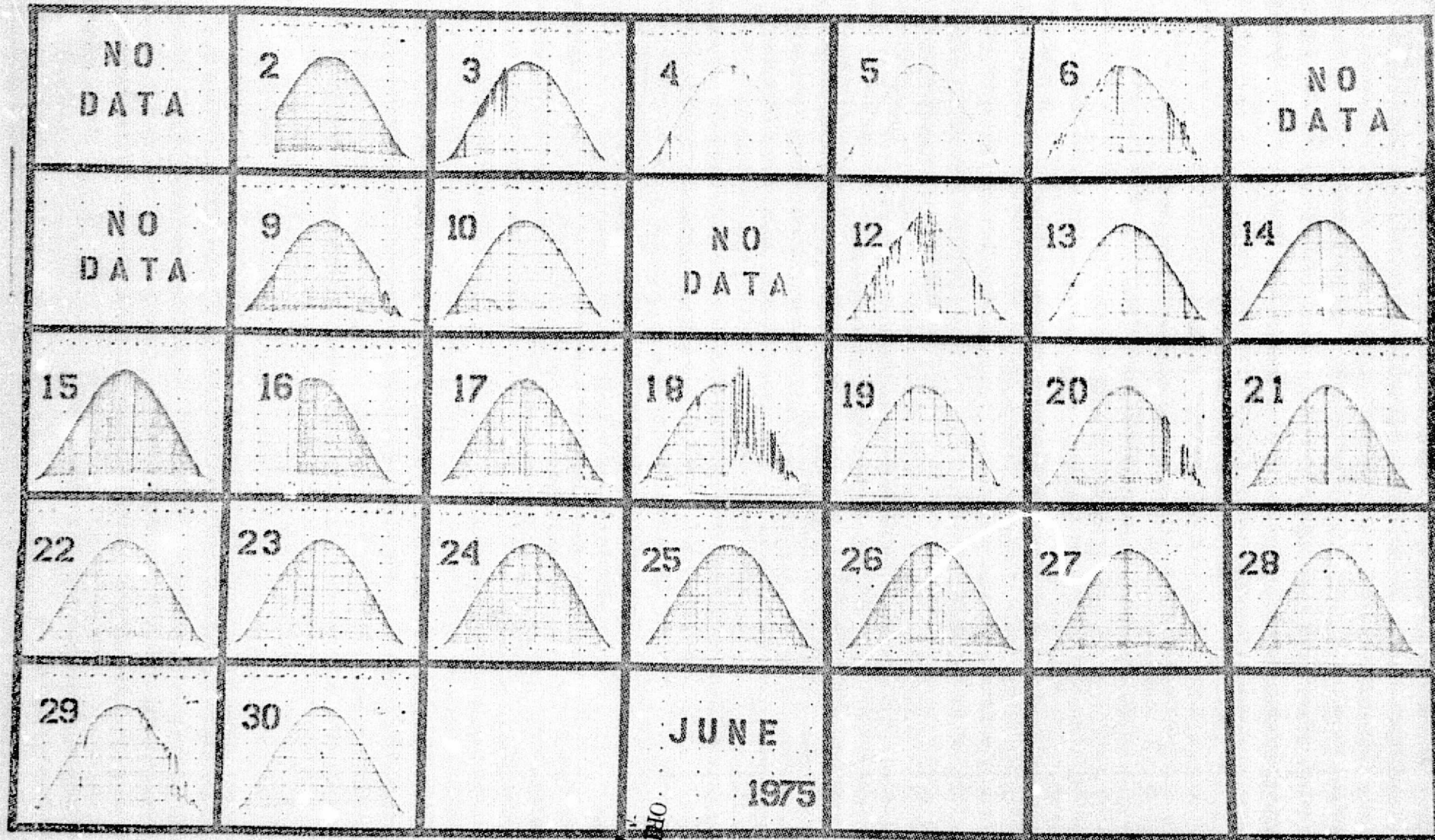
Figure 26.

Figure 27.

APPENDIX II

REFERENCES

1. Meinel, A. B.; McKenney, D.B.; and Beauchamp, W. T.; *"Air Stable Selective Surfaces for Solar Energy Collectors"*, NSF/RANN/SE/GI-41895/PR/74/4.

2. Hildebrandt, A. F. and Vant-Hull, L. L.; *"A Tower Top Focus Solar Energy Collector"*, <u>Mechanical Engineers</u>, Sept. 1974.

3. Ralph, E. L.; *"A Commercial Solar Cell Array Design:,* International Solar Energy Society Conference, NASA/GSFC Greenbelt, Md., May 1971.

APPENDIX III